Guidelines for the design of finite control set model predictive controllers

Guidelines for the Design of Finite Control Set Model Predictive Controllers

Petros Karamanakos, *Senior Member, IEEE*, and Tobias Geyer, *Senior Member, IEEE*

***Abstract*—Direct model predictive control (MPC) with reference tracking, also referred to as finite control set MPC (FCS-MPC), has gained significant attention in recent years, mainly from the academic community. Thanks to its applicability to a wide range of power electronic systems, it is considered a promising control method for such systems. However, to simplify the design, researchers frequently make choices that—often unknowingly—reduce the system performance. We discuss and analyze in this paper the factors that affect the closed-loop performance of FCS-MPC. Based on these findings, design guidelines are provided that help to maximize the system performance. To highlight the performance benefits, two case studies will be considered; the first one consists of a two-level converter and an induction machine, whereas the second one adds an LC filter between the converter and the machine.**

***Index Terms*—Power electronic systems, model predictive control (MPC), direct control, ac drives, integer programming, weighting factors.**

I. Introduction

MODEL predictive control (MPC) [1] was introduced as an advanced control method in the process industry in the 1970s. Formulated in the time domain and suitable for multiple-input multiple-output systems with physical constraints and complex, nonlinear dynamics, MPC was quickly adopted in the petrochemical, chemical, aerospace and automotive industry, to name just a few [2].

Nevertheless, MPC in power electronics has not gained much attention before the early 2000s. Despite some initial research in the 1980s, see, e.g., [3], [4], the lack of sufficient computational power at the time did not allow for further investigations. In recent years, however, the advent of microprocessors with increased computational capabilities renewed the interest of the power electronics community in MPC [5]–[8]. As a result, many algorithms in the framework of MPC have hitherto been developed for several power electronic systems, ranging from low- to high-power applications [9]–[12].

This is reflected by the number of peer-reviewed publications. A search on IEEE *Xplore* with the search term "predictive and control and (inverter or converter)" in the abstract reveals an exponential growth in the number of annual publications, see Fig. 1. Since the year 2000, the number of new publications per year has been roughly doubling every three years.

P. Karamanakos is with the Faculty of Information Technology and Communication Sciences, Tampere University, 33101 Tampere, Finland; e-mail: p.karamanakos@ieee.org

T. Geyer is with ABB Corporate Research, 5405 Baden-Dättwil, Switzerland; e-mail: t.geyer@ieee.org

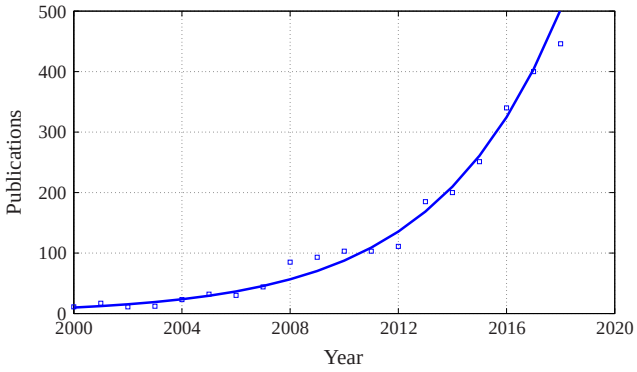

Fig. 1: Annual number of MPC-related peer-reviewed publications appearing in IEEE *Xplore* since 2000. Only publications related to power electronic systems are taken into account.

In academia, direct MPC with reference tracking, also known as finite control set MPC (FCS-MPC), is the favored and most widely published MPC method [13]. This popularity stems from its design simplicity. Specifically, the model of the power electronic system is used to predict its future behavior based on the (finite number of) possible switch positions. The subsequent predictions are assessed on the basis of a chosen optimization criterion (or multiple criteria) that is (are) quantified by an objective function. Following, the switch position that is predicted to provide the most favorable system behavior, i.e., the one that minimizes the objective function, is considered to be optimal. In a last step, the optimal switch position is *directly* applied to the converter without an intermediate modulation stage [14].

As can be understood from the above, the design procedure of FCS-MPC is fairly straightforward. Because of this, researchers advocate the use of FCS-MPC in industry as a superior alternative to established control methods. However, industry is reluctant to adopt new control methods that do not provide significant economic benefits [15]. More specifically, either the investment cost of the power electronic system, i.e., the capital expenditure (CAPEX), or the operating cost, i.e., the operational expenditure (OPEX), need to be reduced. To achieve these benefits with control, it is mandatory to improve some key aspects of the system performance; this, in turn, is typically achieved with more complicated control methods. Indeed, MPC-based algorithms developed in industry are more elaborate and intricate, see, e.g., [16]–[20]. Conversely, the mapping from improved system performance aspects to cost savings must be clearly identified and quantified in order to convince industry to adopt novel MPC methods.

Motivated by the previous observations, this paper focuses

on design guidelines that improve the performance of FCS-MPC. Two major performance metrics will be considered, namely the switching frequency, and the total harmonic distortions (THD) of the load current. The switching frequency relates to the switching losses and, thus, to the converter efficiency. The current THD is a proxy for the harmonic losses in the load. The parameters that affect the system performance, such as the choice of norm, the weighting factors in the objective function, the sampling interval T_s, the length of the prediction horizon, etc., are discussed and analyzed. Subsequently, design guidelines are provided. Moreover, two case studies are used to illustrate the performance benefits—or lack thereof—arising from the design choices, namely a two-level converter driving an induction machine (IM), and the same drive system with an intermediate LC filter.

This paper is structured as follows. The FCS-MPC problem is summarized in Section II. The commonly used terms in the objective function, i.e., the tracking error term and the control effort term, are discussed in Sections III and IV, respectively. Design guidelines for the sampling interval are given in Section V. Section VI analyzes the effect of the prediction horizon, whereas Section VII presents suboptimal designs. Furthermore, a brief performance assessment is provided in Section VIII. Finally, Section IX concludes this paper.

II. Problem Statement

We first review FCS-MPC. In the sequel of this section, the mathematical model of the plant as well as the formulation and solution of the optimal control problem are presented.

A. System Modeling

MPC requires an adequate system model for its predictions. Because MPC is a discrete-time controller, the design of the model has to be done in the discrete-time domain. A generic power electronic system can be described by

$$\boldsymbol{x}(k+1) = \boldsymbol{f}\big(\boldsymbol{x}(k), \boldsymbol{u}(k)\big) \tag{1a}$$

$$\boldsymbol{y}(k) = \boldsymbol{g}\big(\boldsymbol{x}(k)\big)\,, \tag{1b}$$

where $k \in \mathbb{N}$ indicates the discrete time step. The state vector[1] $\boldsymbol{x} \in \mathbb{R}^{n_x}$ in (1) encompasses the variables that fully describe the dynamics of the system in question. Typical state variables in power electronics are the currents flowing through inductors, the voltages across capacitors, the machine fluxes, etc. [14].

The n_y output variables of the system, which are aggregated in the vector $\boldsymbol{y} \in \mathbb{R}^{n_y}$, are a (linear or nonlinear) function of the state variables. Typical output variables are the real and reactive power, electromagnetic torque, flux magnitude, output current, etc. The n_u-dimensional input vector $\boldsymbol{u}$ corresponds to the integer switch positions of the power converter. In the remainder of the paper we consider three-phase systems (i.e., $n_u = 3$); we define the input as $\boldsymbol{u} = \boldsymbol{u}_{abc} = [u_a\ u_b\ u_c]^T$ with

$$\boldsymbol{u} \in \boldsymbol{\mathcal{U}},\ \boldsymbol{\mathcal{U}} \subset \mathbb{Z}^3\,. \tag{2}$$

The extension of the discussion and analysis to systems with $n_u \neq 3$ is straightforward.

In most cases, the power electronic system (1) is a linear system. Thus, the discrete-time state-space model takes the form[2]

$$\boldsymbol{x}(k+1) = \boldsymbol{A}\boldsymbol{x}(k) + \boldsymbol{B}\boldsymbol{K}(\varphi)\boldsymbol{u}(k) \tag{3a}$$

$$\boldsymbol{y}(k) = \boldsymbol{C}\boldsymbol{x}(k)\,. \tag{3b}$$

The system matrix $\boldsymbol{A} \in \mathbb{R}^{n_x \times n_x}$, input matrix $\boldsymbol{B} \in \mathbb{R}^{n_x \times 2}$, and output matrix $\boldsymbol{C} \in \mathbb{R}^{n_y \times n_x}$ are derived based on the system, input and output matrices of the continuous-time state-space model by using some discretization method, most commonly, forward Euler or exact discretization [21].

B. Performance Metrics

The two most relevant metrics to evaluate the system performance are the output current THD I_{THD} and the *average* switching frequency f_{sw} of the converter. The former is defined as

$$I_{\text{THD}} = \frac{\sqrt{\sum_{n\neq 1} \hat{i}_{o,n}^2}}{\hat{i}_{o,1}}\,, \tag{4}$$

where $\hat{i}_{o,n}$ is the amplitude of the load current harmonic at frequency nf_1, with f_1 being the fundamental frequency and $n \in \mathbb{R}^+$.[3] Note that as per definition of the FCS-MPC problem (see Section II-C), minimization of the output current error implies minimization of I_{THD}, see [22, Appendix A].

The average device switching frequency is defined as

$$f_{\text{sw}} = \lim_{M\to\infty} \frac{1}{m c_k M T_s} \sum_{\ell=0}^{M-1} \|\Delta\boldsymbol{u}(\ell)\|_1\,, \tag{5}$$

where $\Delta\boldsymbol{u}(\ell) = \boldsymbol{u}(\ell) - \boldsymbol{u}(\ell-1)$. Moreover, m is the number of the power semiconductor switches of the power converter of interest, and c_k is a converter-dependent "correction" factor such that $\frac{\Delta\boldsymbol{u}}{c_k} \in \{-1, 0, 1\}^3$. For example, $c_k = 2$ for a two-level converter because $u_x \in \{-1, 1\}$, while for a three-level converter we set $c_k = 1$. As discussed in the paper, and according to the FCS-MPC problem in Section II-C, the switching frequency f_{sw} can be controlled directly when the control effort is penalized.

Finally, it is worth mentioning that an insightful performance metric that combines the two aforementioned metrics is their product

$$c_f = I_{\text{THD}} \cdot f_{\text{sw}}\,. \tag{6}$$

[1] Commonly, when three-phase systems are considered, the variables $\boldsymbol{\xi}_{abc} = [\xi_a\ \xi_b\ \xi_c]^T$ in the three-phase (abc) system are mapped into a two-dimensional orthogonal space. The latter can either be rotating with the angular speed ω_{fr} (referred to as the dq-plane), or be stationary, i.e., $\omega_{\text{fr}} = 0$ (referred to as the $\alpha\beta$-plane). For mapping to the dq-plane the transformation $\boldsymbol{\xi}_{dq} = \boldsymbol{K}(\varphi)\boldsymbol{\xi}_{abc}$, with $\boldsymbol{\xi}_{dq} = [\xi_d\ \xi_q]^T$ and φ being the angle between the d- and the a-axis, is performed. When the mapping is done to the $\alpha\beta$-plane, the transformation is of the form $\boldsymbol{\xi}_{\alpha\beta} = \boldsymbol{K}(0)\boldsymbol{\xi}_{abc}$, with $\boldsymbol{\xi}_{\alpha\beta} = [\xi_\alpha\ \xi_\beta]^T$.

[2] Hereafter, we drop the subscript from variables in the abc-plane to simplify the notation, whereas variables in the $\alpha\beta$- and dq-plane are denoted with the corresponding subscript.

[3] An alternative metric for the current distortions is the current total demand distortion (TDD). The difference with I_{THD} is that the nominal peak output current constitutes the denominator in (4). The main benefit of such a metric is that the current TDD does not approach infinity when the fundamental component $\hat{i}_{o,1}$ is zero. However, when operation at nominal conditions is considered—as in the cases considered in this paper—the current THD and TDD are the same.

This metric quantifies the product of the current distortions and switching frequency, and thus the quality of the control and modulation scheme in question; c_f being approximately constant defines a hyperbolic trade-off between I_{THD} and f_{sw}. Therefore, a lower c_f implies a higher performing control method at steady-state operation.

C. FCS-MPC Problem

Consider the sequence of manipulated variables over a finite horizon of $N_p \in \mathbb{N}^+$ time steps

$$\boldsymbol{U}(k) = \Big[\boldsymbol{u}^T(k) \;\; \boldsymbol{u}^T(k+1) \;\; \ldots \;\; \boldsymbol{u}^T(k+N_p-1)\Big]^T \in \mathbb{U}\,, \tag{7}$$

where $\mathbb{U} = \boldsymbol{\mathcal{U}}^{N_p}$. With $\boldsymbol{U}(k)$ and the present state $\boldsymbol{x}(k)$ the future behavior of the power electronic system can be predicted over the prediction horizon with the help of (1) (or (3)).

The control objectives are quantified and mapped into a non-negative scalar value via the objective function $J : \mathbb{R}^{n_x} \times \mathbb{U} \to \mathbb{R}^+$, which is of the form[4]

$$J\big(\boldsymbol{x}(k), \boldsymbol{U}(k)\big) = \sum_{\ell=k}^{k+N_p-1} J^\dagger\big(\boldsymbol{x}(\ell+1), \boldsymbol{u}(\ell)\big)\,. \tag{8}$$

The stage cost $J^\dagger(\star)$ is commonly based either on the ℓ_1-norm or the ℓ_2-norm. Consider the n-dimensional vector $\boldsymbol{\xi} = [\xi_1 \;\; \xi_2 \;\; \ldots \;\; \xi_n]^T$. The ℓ_1-norm is defined as

$$\|\boldsymbol{\xi}\|_1 = |\xi_1| + |\xi_2| + \ldots + |\xi_n|\,,$$

where $|\star|$ denotes the absolute value of a scalar quantity. The squared ℓ_2-norm is given as

$$\|\boldsymbol{\xi}\|_2^2 = \xi_1^2 + \xi_2^2 + \ldots + \xi_n^2 = \boldsymbol{\xi}^T\boldsymbol{\xi}\,.$$

Because the control problem is formulated as a reference tracking problem [9], the output variables $\boldsymbol{y}$ must track their references $\boldsymbol{y}_{\mathrm{ref}}$. This is captured by the stage cost

$$J^\dagger\big(\boldsymbol{x}(\ell+1), \boldsymbol{u}(\ell)\big) = \|\boldsymbol{y}_{\mathrm{ref}}(\ell+1) - \boldsymbol{y}(\ell+1)\|_p^p + \lambda_u \|\Delta\boldsymbol{u}(\ell)\|_p^p\,, \tag{9}$$

with $p \in \{1, 2\}$. The output tracking error and the control effort are penalized at each time step. Note that the difference between two consecutive switch positions $\Delta\boldsymbol{u}(\ell)$ is penalized rather than the switch position itself. This allows one to control the average switching frequency f_{sw} of the converter. Finally, the non-negative weighting factor $\lambda_u \in \mathbb{R}^+$ adjusts the trade-off between the two aforementioned terms.

[4] An alternative form of the objective function is

$$J\big(\boldsymbol{x}(k), \boldsymbol{U}(k)\big) = P\big(\boldsymbol{x}(k+N_p)\big) + \sum_{\ell=k}^{k+N_p-1} J^\dagger\big(\boldsymbol{x}(\ell), \boldsymbol{u}(\ell)\big)\,,$$

where $P(\star)$ describes the cost at the terminal state. This terminal cost can be used to ensure closed-loop stability [1], [23].

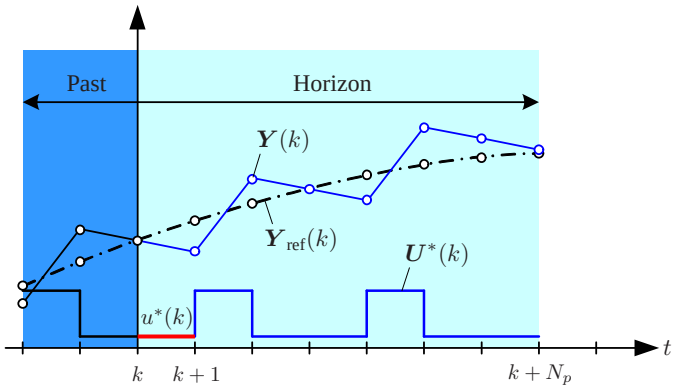

(a) Horizon at time step k

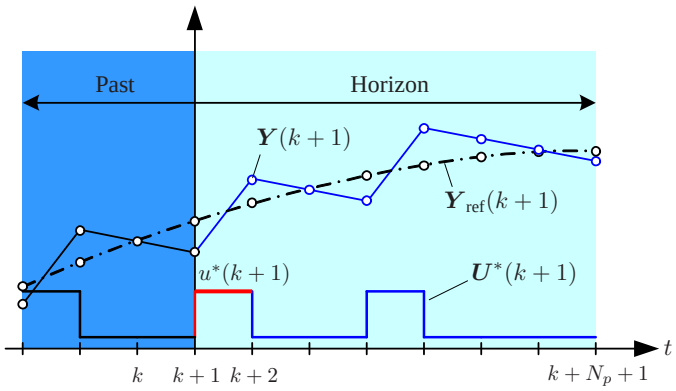

(b) Horizon at time step $k+1$

Fig. 2: Receding horizon policy for a six-step prediction horizon ($N_p = 6$). For simplicity, a single-input single-output (SISO) system is assumed. The predicted output and output reference trajectories are denoted with $\boldsymbol{Y}(k) = [y(k+1) \;\; \ldots \;\; y(k+N_p)]^T$ and $\boldsymbol{Y}_{\mathrm{ref}}(k) = [y_{\mathrm{ref}}(k+1) \;\; \ldots \;\; y_{\mathrm{ref}}(k+N_p)]^T$, respectively.

D. Integer Optimization Problem

Based on the objective function (8), the system model (1), the (integer) input constraint (2), and (optional) explicit state constraints of the form $\boldsymbol{x}(k) \in \boldsymbol{\mathcal{X}} \subseteq \mathbb{R}^{n_x}$, the integer optimization problem is formulated as

$$\begin{aligned} \underset{\boldsymbol{U}(k)}{\text{minimize}} \quad & J\big(\boldsymbol{x}(k), \boldsymbol{U}(k)\big) \\ \text{subject to} \quad & \boldsymbol{x}(\ell+1) = \boldsymbol{f}\big(\boldsymbol{x}(\ell), \boldsymbol{u}(\ell)\big) \\ & \boldsymbol{y}(\ell+1) = \boldsymbol{g}\big(\boldsymbol{x}(\ell+1)\big) \\ & \boldsymbol{u}(\ell) \in \boldsymbol{\mathcal{U}} \\ & \boldsymbol{x}(\ell+1) \in \boldsymbol{\mathcal{X}} \;\; \forall\, \ell = k, \ldots, k+N_p-1\,. \end{aligned} \tag{10}$$

The optimization problem (10) is often solved by using the brute-force approach of exhaustive enumeration [8]. To reduce the computational load, methods that rely on dedicated optimization algorithms such as branch-and-bound [24], and non-trivial prediction horizon formulations [25] should be considered. The solution of (10) is the open-loop *optimal* sequence of manipulated variables

$$\boldsymbol{U}^*(k) = \Big[\boldsymbol{u}^{*T}(k) \;\; \boldsymbol{u}^{*T}(k+1) \;\; \ldots \;\; \boldsymbol{u}^{*T}(k+N_p-1)\Big]^T\,. \tag{11}$$

Out of this sequence only the first element $\boldsymbol{u}^*(k)$ is applied to the converter, whereas the rest are discarded. Following,

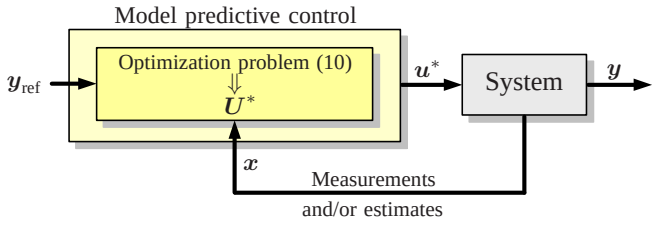

Fig. 3: FCS-MPC with output reference tracking.

problem (10) is solved over a horizon shifted by one time step using new measurements and/or estimates. This so-called *receding horizon* policy provides feedback to the MPC algorithm; this concept is visualized in Fig. 2. The block diagram of FCS-MPC with output reference tracking is shown in Fig. 3.

The optimization problem in (10) simplifies significantly when adopting the ℓ_2-norm in the objective function (8), considering the linear discrete-time model (3) and removing the constraints by setting $\boldsymbol{u} \in \mathbb{R}^3$ and $\boldsymbol{x} \in \mathbb{R}^{n_x}$. The optimization problem is then a convex quadratic program (QP) with linear equality constraints. Its so-called *unconstrained solution*

$$\boldsymbol{U}_{\text{unc}}(k) = \begin{bmatrix} \boldsymbol{u}_{\text{unc}}^T(k) & \boldsymbol{u}_{\text{unc}}^T(k+1) & \dots & \boldsymbol{u}_{\text{unc}}^T(k+N_p-1) \end{bmatrix}^T \tag{12}$$

can be found by setting the gradient of (8) equal to zero, i.e.,

$$\nabla J\big(\boldsymbol{x}(k), \boldsymbol{U}(k)\big) = \boldsymbol{0}\,, \tag{13}$$

where the components of $\nabla J(\star) \in \mathbb{R}^{3N_p}$ are the partial derivatives of $J(\star)$

$$\nabla J\big(\boldsymbol{x}(k), \boldsymbol{U}(k)\big)_i = \frac{\partial J\big(\boldsymbol{x}(k), \boldsymbol{U}(k)\big)}{\partial u_i(k)}\,,\ i = 1, \dots, 3N_p\,.$$

The unconstrained solution (12) will be utilized in several ways later in this paper.

III. Tracking Error

This section is dedicated to the design of the tracking error term (9) in the objective function. In the sequel, the most common pitfall—namely a poorly chosen norm—is discussed, which can lead to suboptimal performance or even instability. Moreover, tuning guidelines are provided that can improve the system performance.

A. Choice of Norm

The computation of the stage cost (9) is computationally cheaper when the ℓ_1-norm—instead of the ℓ_2-norm—is used. Therefore, from a computational perspective, the adoption of the ℓ_1-norm in FCS-MPC seems to be preferable, particularly in light of the fact that the MPC algorithm has to be executed in real time within a few tens of microseconds. As a result, the MPC problem is often based on the ℓ_1-norm in the literature, see, e.g., [8], [26]–[41].

Focusing on this issue, a detailed analysis of the choice of norm in FCS-MPC is presented in [42]. Therein, it is shown that when the ℓ_2-norm is used in (9), i.e.,

$$J^\dagger\big(\boldsymbol{x}(\ell+1), \boldsymbol{u}(\ell)\big) = \|\boldsymbol{y}_{\text{ref}}(\ell+1) - \boldsymbol{y}(\ell+1)\|_2^2 + \lambda_u \|\Delta \boldsymbol{u}(\ell)\|_2^2\,,$$

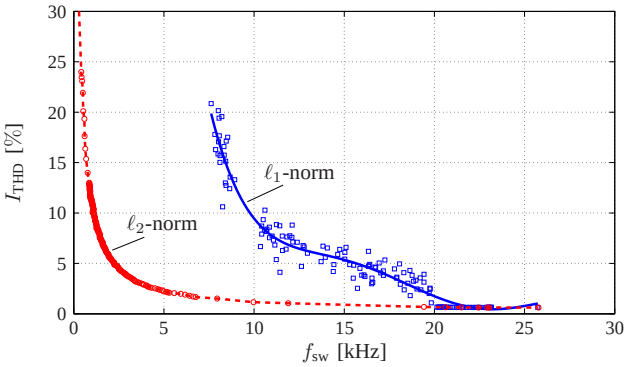

Fig. 4: Trade-off curves for the stage cost (9) with ℓ_1- and ℓ_2-norm. The current THD I_{THD} is shown for the achievable range of switching frequencies f_{sw}. The solid (blue) and dashed (red) lines are polynomial approximations of the individual simulation results. The individual simulations are indicated by squares and circles for current FCS-MPC based on the ℓ_1- and ℓ_2-norm, respectively.

closed-loop (practical) stability[5] of the system is guaranteed [43]. On the other hand, the ℓ_1-norm can result in a performance deterioration as well as closed-loop instability, provided that $\lambda_u \neq 0$. For $\lambda_u = 0$, stability issues do not arise, but setting the penalty on the control effort to zero is not recommended, as will be explained in Section IV.

Besides the stability issues incurred by the use of the ℓ_1-norm in (9), a limited range of switching frequencies as well as performance degradation are among the direct consequences of such a design choice. To show this consider a two-level inverter driving an IM (this case study is presented in Appendix A). Let FCS-MPC control the stator current $\boldsymbol{i}_{s,\alpha\beta}$ of the system, i.e., $\boldsymbol{y} = \boldsymbol{i}_{s,\alpha\beta}$. We set the sampling interval to $T_s = 5\,\mu$s. The stator current THD, I_{THD}, is plotted versus the average device switching frequency f_{sw} in Fig. 4.

When the ℓ_2-norm is used and λ_u is varied between 0 and 0.025, a wide range of switching frequencies is achieved. The highest switching frequency occurs for $\lambda_u = 0$ and, thus, depends only on the chosen sampling interval. The lowest possible switching frequency occurs in six-step operation; to achieve this, we set $\lambda_u = 0.025$. On the other hand, when the objective function is based on the ℓ_1-norm, stability is lost when λ_u exceeds 0.0163. Operation at low switching frequencies is, thus, not possible, as can be seen in Fig. 4. For a detailed discussion of these findings, the interested reader is referred to [42].

Thanks to Parseval's identity the ℓ_2-norm of a signal corresponds to its energy [44]. In the context of power electronics, the ℓ_2-norm of a ripple variable is proportional to its THD, see [22, Appendix A]. Therefore, minimizing the output tracking error $\boldsymbol{y}_{\text{ref}} - \boldsymbol{y}$ is akin to minimizing the THD of the output variables $\boldsymbol{y}$. This implies that better tracking performance is achieved when the ℓ_2-norm is used in (9). This can be seen in Fig. 4, where for the shown range of achievable switching frequencies, the performance of FCS-MPC based on the ℓ_1-norm is equal to or worse than that of FCS-MPC with the ℓ_2-norm. This observation leads to the first guideline.

[5]For the definition of practical stability the reader is referred to [23, Section II] and references therein.

Design guideline 1. *The stage cost should be based on the ℓ_2-norm by setting $p = 2$ in* (9)*. By doing so, practical closed-loop stability, favorable tracking performance and comparatively low distortions are ensured.*

B. Algebraic Tuning Guidelines

The output current of the converter, regardless of whether it is fed into the grid, an electrical machine, or any other load, should have as low a THD as possible. To this aim, the straightforward approach is to directly control it, i.e., to define it as an output variable $\boldsymbol{y}$ so as to regulate it with the help of (9) along its reference $\boldsymbol{y}_{\text{ref}}$. Within the family of FCS-MPC methods, current FCS-MPC minimizes the current THD for a given switching frequency, as shown in [22].

Nevertheless, for grid-connected converters, it is sometimes preferable to directly control the real and reactive power. Similarly for electrical machines, the electromagnetic torque and the stator flux magnitude are of prime interest and often defined as output variables. This implies that a weighting factor is required that sets the relative importance between the two output variables. When controlling the real and reactive power, the penalty on the corresponding two error tracking terms should be equal [27], [45], [46]; a related discussion can be found in [14, Section 11.3.3] for model predictive direct power control. Heuristically tuning the weighting factor for torque and flux control, or simply assigning the same weight to the two objective function terms, as done, e.g., in [41], [47], [48], is a questionable practice. In general, the current THD and, thus, the closed-loop performance deteriorates.

As shown in [22], a closed-form expression for the weighting factor in model predictive torque and flux control can be derived. This is done by designing the objective function of the problem in question such that its level sets are similar to those of the current control problem. As a result, the flux/torque controller produces very *similar* current distortions per switching frequency to those of the predictive current controller. Going one step further, the flux/torque controller achieves the *same* current THD as the predictive current controller when replacing the stator flux by the rotor flux in the objective function (of the flux/torque controller) [49].

Consider again the two-level inverter drive system described in Appendix A, and assume operation at nominal speed and rated torque. Fig. 5 shows simulation results that highlight the equivalence between the two control methods.

Design guideline 2. *To achieve similar current distortions for current FCS-MPC and torque/flux FCS-MPC, the weighting factor introduced in the output tracking error term* (9) *of the latter can be set based on an analytical expression. Tuning is avoided.*

IV. Penalty on the Control Effort

The effect of the control effort weighting factor λ_u on the system performance is analyzed in this section. Two cases are examined, i.e., $\lambda_u = 0$ and $\lambda_u > 0$. The relevant performance benefits, or lack thereof, are discussed, and design guidelines are proposed.

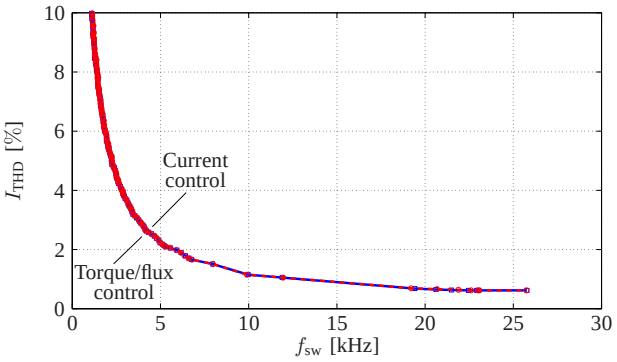

Fig. 5: Trade-off between current THD I_{THD} and switching frequency f_{sw} for current FCS-MPC (solid, blue line), and torque/flux FCS-MPC (dashed, red line). The individual simulations are shown as squares (current control), and circles (torque/flux control).

A. Similarity with Deadbeat Control

Deadbeat control is a control technique that aims to eliminate the tracking error at the end of the sampling interval T_s provided that the system is one-step reachable [50].[6] This is achieved by computing the appropriate modulating signal $\boldsymbol{u}_{\text{db}} \in [-1, 1]^3 \subset \mathbb{R}^3$ which is fed into a modulator. Therefore, deadbeat controllers show fast dynamic responses, but also poor robustness to model mismatches and parameter uncertainties [51], [52].

For $\lambda_u = 0$, FCS-MPC resembles the behavior of deadbeat control, as explained in the following. This holds true regardless of whether a short or a long prediction horizon is used.

1) One-Step FCS-MPC: As can also be seen in [12, Table III], the most common implementation of FCS-MPC considers a one-step prediction horizon ($N_p = 1$), and the stage cost does not include the control effort term $\Delta\boldsymbol{u}$ (or equivalently $\lambda_u = 0$), see, e.g., [8], [27]–[32], [34]–[41], [47], [53]–[55]. With such a design, the objective function simplifies to

$$J\big(\boldsymbol{x}(k), \boldsymbol{u}(k)\big) = \|\boldsymbol{y}_{\text{ref}}(k+1) - \boldsymbol{y}(k+1)\|_2^2\,, \tag{14}$$

where only the ℓ_2-norm is considered for the reasons explained in Section III-A.

Theorem 1. *Consider a three-phase power electronic system described by the linear state-space model* (3)*. One-step FCS-MPC without penalization of the control effort (as* (14)*) is a quantized deadbeat controller.*

Proof. The proof is provided in [56, Section 3]. ■

In other words, according to Theorem 1, the deadbeat solution $\boldsymbol{u}_{\text{db}}$ is the same as the *unconstrained* (i.e., relaxed) solution $\boldsymbol{u}_{\text{unc}}$ of the optimization problem (10), see (12). With one-step FCS-MPC, however, $\boldsymbol{u}_{\text{unc}}$ cannot be synthesized by a subsequent PWM stage because the switch positions are directly manipulated. Therefore, the concept of deadbeat control is extended; the solution of the FCS-MPC problem is

[6] This is the case for first-order systems without input constraints. For systems of order $\ell > 1$, reachability can be achieved in ℓ time steps. Without loss of generality, the concepts discussed hereafter can be directly extended and applied to such systems as well.

the three-phase switch position $\boldsymbol{u}$ that minimizes the tracking error at the next time step, regardless of the switching effort. As a consequence, MPC with objective function (14) can be interpreted as a quantized deadbeat control technique which inherits the corresponding performance characteristics, as mentioned at the beginning of this section.

2) Multistep FCS-MPC: Although, as will be analyzed in Section VI, long prediction horizons offer performance benefits, a common belief in the power electronic community is that they are not necessary. This misconception stems from the poor formulation of the MPC problem, i.e., the lack of the control effort penalization. Thereby, for long-horizon FCS-MPC with $N_p > 1$ and $\lambda_u = 0$, the function to be minimized is of the form

$$J\big(\boldsymbol{x}(k), \boldsymbol{U}(k)\big) = \sum_{\ell=k}^{k+N_p-1} \|\boldsymbol{y}_{\text{ref}}(\ell+1) - \boldsymbol{y}(\ell+1)\|_2^2 \,. \quad (15)$$

MPC with (15), nonetheless, resembles a deadbeat controller, as stated in the following theorem.

Theorem 2. *Consider a three-phase power electronic system described by the linear state-space model* (3)*. Multistep FCS-MPC without penalization of the control effort (see function* (15)*) is a quantized deadbeat controller.*

Proof. The proof is provided in Appendix C. ■

Therefore, long-horizon FCS-MPC with the objective function (15) cannot improve the system performance as compared with one-step horizon MPC with function (14) because both methods produce exactly the same control actions.

3) Performance: The similarity between FCS-MPC with $\lambda_u = 0$ and quantized deadbeat control implies that the features that characterize the latter control method are inherited by the former. This means that FCS-MPC shows favorable dynamic operation, but inferior steady-state performance compared with conventional modulation techniques.

More specifically, owing to the lack of the control effort penalization, the switching frequency in FCS-MPC is limited only by the chosen sampling interval T_s. Although the theoretical maximum switching frequency is equal to $f_{\text{sw}} = f_s/2$, with $f_s = 1/T_s$ being the sampling frequency, empirical studies show that it is less than $f_s/4$ [13, Chapter 4]; this is also implied by Fig. 4, for which we have $f_{\text{sw}} \approx f_s/7.7$.

When operating the converter at the highest possible switching frequency (with $\lambda_u = 0$), FCS-MPC does not outperform conventional methods, such as space vector modulation (SVM) [57]. This is shown in Table I, where a comparison between one-step FCS-MPC, multistep FCS-MPC, and SVM is presented. We consider again current control of the two-level drive system in Appendix A. A switching frequency of $f_{\text{sw}} \approx 2.3\,\text{kHz}$ results when setting the sampling interval to $T_s = 50\,\mu\text{s}$, regardless of the length of the prediction horizon. Clearly, the current distortions are also the same for the one-step and the multistep FCS-MPC. To achieve the same switching frequency for SVM, the modulation cycle is chosen as $T_c = 434.78\,\mu\text{s}$. Note that its current distortions are slightly lower. A similar result is obtained at the switching frequency $f_{\text{sw}} \approx 25.75\,\text{kHz}$, see Table I.

TABLE I: Current THD I_{THD} of a two-level drive system (see Appendix A) when operated either at $f_{\text{sw}} \approx 2.3\,\text{kHz}$ or at $f_{\text{sw}} \approx 25.75\,\text{kHz}$.

Control scheme	Control settings	f_{sw} [kHz]	I_{THD} [%]
SVM	$T_c = 434.78\,\mu\text{s}$	2.3	5.99
MPC	$N_p = 1$, $\lambda_u = 0$, $T_s = 50\,\mu\text{s}$		6.04
MPC	$N_p = 10$, $\lambda_u = 0$, $T_s = 50\,\mu\text{s}$		6.04
SVM	$T_c = 38.84\,\mu\text{s}$	25.75	0.56
MPC	$N_p = 1$, $\lambda_u = 0$, $T_s = 5\,\mu\text{s}$		0.62
MPC	$N_p = 10$, $\lambda_u = 0$, $T_s = 5\,\mu\text{s}$		0.62

Design guideline 3. *The control effort in FCS-MPC must always be penalized to ensure acceptable current distortions per switching frequency.*

As will be explained in Section V, a high sampling-to-switching-frequency ratio is required to ensure an acceptable steady-state performance. To enable a high ratio, the control effort must be penalized with the aim to reduce the switching frequency. Lowering the switching frequency by increasing the sampling interval, however, leads to a low sampling-to-switching-frequency ratio and, thus, to rather high current distortions per switching frequency. FCS-MPC then also resembles deadbeat control, which is characterized by a high sensitivity to measurement and observer noise.

B. Tuning of the Weighting Factor on the Control Effort

The objective function (8) comprises two competing scalar terms that are to be minimized. To prioritize among the two terms, the weighing factor λ_u is introduced; this parameter needs to be tuned such that the desired performance is achieved. The standard practice is to tune the weighting factor manually.

More generally, the optimization problem (10) is, by definition, a multi-criterion optimization problem with trade-off curves or surfaces [58, Section 4.7]. It is common practice to explore the so-called Pareto optimal points, i.e., these feasible points that are "better" from an optimization perspective than all other feasible points. Owing to the non-convex nature of the integer optimization problem, however, the trade-off surfaces are not monotonic, see also Figs. 4 and 5. Because of that, the tuning process becomes more difficult; this fact was also pointed out in [59], wherein a first discussion on how to empirically design such parameters was presented. Some more laborious ways to choose the weights have been recently proposed, see, e.g., [60], [61].

C. Alternative Approaches

To avoid the difficulties discussed above, a promising approach was recently proposed in [62]. The minimization of the weighted control effort is replaced by a new term that penalizes the predicted deviation of the switching frequency from its reference. More specifically, the stage cost (9) is rewritten as

$$J^{\dagger}\big(\boldsymbol{x}(\ell+1), \boldsymbol{u}(\ell)\big) = \|\boldsymbol{y}_{\text{ref}}(\ell+1) - \boldsymbol{y}(\ell+1)\|_p^p + \lambda_u \|f_{\text{sw,ref}}(\ell+1) - \hat{f}_{\text{sw}}(\ell+1)\|_p^p \,; \quad (16)$$

the switching effort term $\|\Delta \boldsymbol{u}(\ell)\|_p^p$ is replaced with the tracking term $\|f_{\text{sw,ref}}(\ell+1) - \hat{f}_{\text{sw}}(\ell+1)\|_p^p$. This term introduces the desired operating switching frequency $f_{\text{sw,ref}}$ as well as the *predicted* switching frequency $\hat{f}_{\text{sw}}$. With regard to the latter, a filter can be used to capture the switching frequency f_{sw} as defined in (5). To this aim, e.g., a second-order infinite impulse response (IIR) filter was proposed in [62]. Depending on the state of this filter and the switching sequence $\boldsymbol{U}(k)$, the approximate switching frequency over the prediction horizon can be predicted.

To avoid the tuning of the control effort altogether, one can formulate an MPC problem in which the switching frequency is fixed and directly defined by the chosen sampling interval T_s. This can be done by choosing the number of possible switching transitions within a given time interval. Starting with [63], several related methods have been proposed, see, e.g., [64]–[72]. The objective function is simplified, thus allowing the controller to focus only on the tracking of the output reference $\boldsymbol{y}_{\text{ref}}$. This significantly simplifies the tuning procedure. However, because these problem formulations do not meet the problem definition in (10), they differ from FCS-MPC methods and are, thus, out of the scope of this paper.

Design guideline 4. *The weighting factors in multi-criterion optimization problems such as* (10) *are most commonly tuned by exploring the associated trade-off surfaces. This renders the tuning procedure cumbersome. To avoid this, one could fix the switching frequency while FCS-MPC focuses on minimizing the tracking error.*

V. Sampling Interval

FCS-MPC restricts switching transitions to the discrete time instants $kT_s, (k+1)T_s, \ldots$. This fact directly follows from the formulation of the optimization problem in (10), which leads to a constant switch position in the interval $[kT_s, (k+1)T_s]$. The discretization of the time axis is required to formulate and solve the MPC problem in the discrete-time domain, but the restriction of switching to discrete-time steps is unique to FCS-MPC.

A key metric is the ratio between the sampling frequency and the switching frequency. This ratio defines the *granularity of switching*. More specifically, a low sampling-to-switching-frequency ratio unduly restricts the switching instants of FCS-MPC to a coarsely sampled time axis. This is illustrated in Fig. 6(a), which shows a single-phase switching sequence for the low sampling-to-switching-frequency ratio of 10. On the other hand, a high sampling-to-switching-frequency ratio allows FCS-MPC to switch at approximately any moment in time, and, thus, effectively in the continuous-time domain. This results in a fine granularity of switching. Fig. 6(b) shows a switching sequence for the high sampling-to-switching-frequency ratio of 100.

As a rule of thumb, the sampling frequency f_s should be about two orders of magnitude higher than the switching frequency f_{sw} [62], [73]–[78]. Such a high ratio is required for all direct control techniques. Industrial drives controlled by direct torque control (DTC) [79], e.g., require a sampling frequency of $40\,\text{kHz}$ when operating at switching frequencies

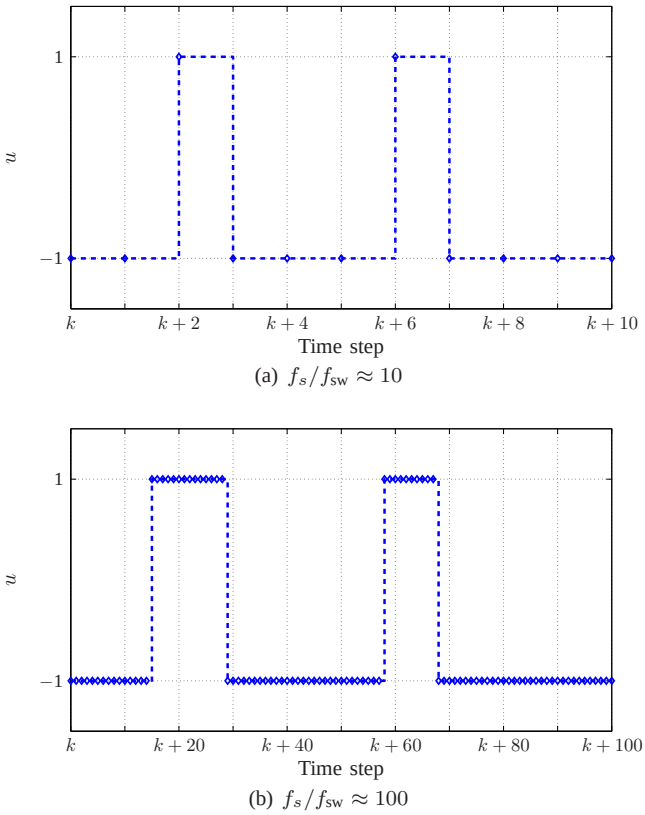

(a) $f_s/f_{\text{sw}} \approx 10$

(b) $f_s/f_{\text{sw}} \approx 100$

Fig. 6: Single-phase switching sequence for switching frequency at about $500\,\text{Hz}$. The sampling frequency is (a) $5\,\text{kHz}$, and (b) $50\,\text{kHz}$. The individual samples are shown as rhombi. The time window corresponds to $2\,\text{ms}$.

TABLE II: Current THD I_{THD} of a two-level converter when operating at $f_{\text{sw}} = 4\,\text{kHz}$.

Control scheme	Control settings	f_s/f_{sw}	I_{THD} [%]
SVM	$f_c = 4\,\text{kHz}$	—	1.67
MPC	$\lambda_u = 0$, $T_s = 35\,\mu\text{s}$	7.14	2.06
MPC	$\lambda_u = 5 \cdot 10^{-6}$, $T_s = 30\,\mu\text{s}$	8.33	1.79
MPC	$\lambda_u = 3.1 \cdot 10^{-4}$, $T_s = 20\,\mu\text{s}$	12.5	1.75
MPC	$\lambda_u = 1.9 \cdot 10^{-4}$, $T_s = 10\,\mu\text{s}$	25	1.59
MPC	$\lambda_u = 1.2 \cdot 10^{-4}$, $T_s = 5\,\mu\text{s}$	50	1.56
MPC	$\lambda_u = 6.5 \cdot 10^{-5}$, $T_s = 2.5\,\mu\text{s}$	100	1.51
MPC	$\lambda_u = 2.7 \cdot 10^{-5}$, $T_s = 1\,\mu\text{s}$	250	1.47
MPC	$\lambda_u = 7 \cdot 10^{-6}$, $T_s = 0.25\,\mu\text{s}$	1000	1.47

of up to $250\,\text{Hz}$ to achieve the desired steady-state behavior as well as a superior dynamic performance [80].

To confirm this rule of thumb, consider a two-level converter with an active RL load operating at rated power. One-step current FCS-MPC is used with various sampling intervals. The penalty on switching, λ_u, is adjusted accordingly to achieve a switching frequency of $4\,\text{kHz}$. The results are summarized in Table II, where SVM is used as a baseline using the same switching frequency.

The table indicates that a sampling-to-switching-frequency ratio of at least 20 is required to outperform SVM. Ratios in excess of 50 can further improve the steady-state performance, although less significantly. The table also confirms that setting the penalty on switching to zero and using the sampling

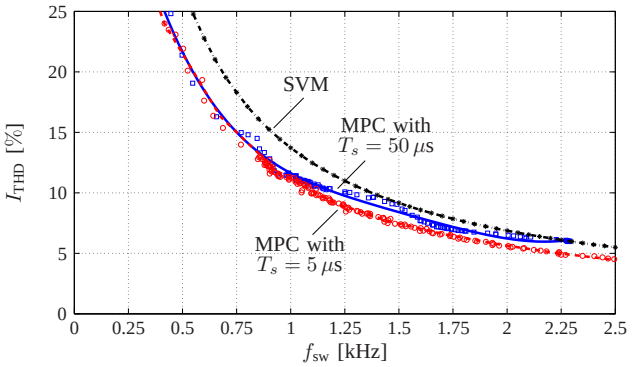

Fig. 7: Trade-off between current THD I_{THD} and switching frequency f_{sw} for FCS-MPC with $T_s = 50\,\mu$s (solid, blue line), FCS-MPC with $T_s = 5\,\mu$s (dashed, red line), and SVM (dash-dotted, black line). The individual simulations are shown as squares (MPC with $T_s = 50\,\mu$s), circles (MPC with $T_s = 5\,\mu$s), and asterisks (SVM).

interval as a tuning parameter to set the switching frequency is a poor design choice, leading to much higher current distortions than SVM. Even though this is common practice, see, e.g., [8], [27], [31], [34]–[41], [47], [53], [54], [81]–[83], it is not recommended.

The benefit of high sampling-to-switching-frequency ratios can also be observed in Fig. 7. Considering the two-level drive system of Appendix A, the performance of one-step current FCS-MPC in terms of current distortions is depicted for $T_s = 5\,\mu$s and $50\,\mu$s. When low switching frequencies are desired then both sampling intervals perform equally well because the ratio f_s/f_{sw} is high. However, as the switching frequency increases, the current THD produced by MPC with the long sampling interval becomes worse than that of MPC with the short sampling interval, when the sampling-to-switching-frequency ratio falls below 25.

Design guideline 5. *To ensure a fine granularity of switching in FCS-MPC, the sampling frequency should be two orders of magnitude higher than the switching frequency (and a penalty on the switching transitions should be imposed to achieve the desired the switching frequency).*

To achieve high sampling frequencies, control platforms based on field-programmable gate array (FPGA) are well suited, because operations can be highly pipelined and parallelized [62], [84]. Alternatively, discrete-time control methods should be considered that facilitate switching at any moment in time within the sampling interval. Two examples for this include [16] and [71], but more research effort is required to develop MPC methods for converters operating at high switching frequencies.

VI. Length of the Prediction Horizon

It is a common misconception that solving the integer optimization problem (10) is numerically easy and that it can be done in a straightforward manner with exhaustive enumeration. Indeed, problem (10) underlying MPC is inherently difficult to solve as it is known to be NP-hard. This means that its computational complexity increases exponentially with the dimension of the optimization vector, i.e., the switching sequence $\boldsymbol{U}(k)$. Hence, (10) can quickly become computationally intractable as the length of the horizon increases.

A common practice to keep the computational complexity at bay is to choose as short a prediction horizon as possible; in almost all cases, $N_p = 1$ is selected [10]. However, it is well-known that a long prediction horizon can improve the closed-loop stability margin as well as the plant performance in MPC [85]. In the case of FCS-MPC with reference tracking for power electronics this was confirmed in [86]. Therefore, a trade-off between control performance and computational complexity arises. In the sequel of this section the benefits of long horizons are examined for a first- and a third-order system.

A. First-Order System

The effect of the longer horizon on the system performance is shown in Fig. 8 for the two-level drive system (see Appendix A). The sampling interval is set to $T_s = 5\,\mu$s. As can be observed, long-horizon FCS-MPC outperforms one-step MPC over the whole range of the shown switching frequencies. Long horizons are particularly beneficial for switching frequencies below 1 kHz, see Fig. 8(b). The relative *improvement* in the current THD

$$I_{\text{THD,rel}} = \left| \frac{I_{\text{THD}}|_{N_p=10} - I_{\text{THD}}|_{N_p=1}}{I_{\text{THD}}|_{N_p=1}} \right| ,$$

peaks at approximately $\approx 12\%$ for the switching frequency $f_{\text{sw}} = 500\,\text{Hz}$. This is a notable, but relatively modest performance improvement. Larger gains of about 20% can be achieved for three-level converters, see [86].

The absence of a considerable performance benefit is due to the simplicity of the chosen system. The transfer function from the switch position (i.e., the manipulated variable) to the output current (i.e., the controlled variable) is a first-order system, one in each axis of the stationary orthogonal coordinate system. First-order systems, are, in general, easy to control, and thus more sophisticated and complex control methods—such as long-horizon MPC—provide only minor performance benefits.

Design guideline 6. *For first-order systems, long horizons offer modest performance benefits over a limited range of operating points and switching frequencies. Therefore, a short horizon typically suffices.*

B. Third-Order System

When higher-order systems, such as converters with LC or LCL filters, are the targeted applications, long horizons strongly impact the closed-loop performance [87]. Due to the more complex dynamics of such systems, a long prediction horizon enables the controller to make better educated decisions because the evolution of the system state is computed over a longer time interval into the future.

This performance boost is also visible in Fig. 9. A third-order system is considered, namely the aforementioned two-level drive system with an LC filter and a resonance frequency of $830\,\text{Hz}$, see Appendix B. The sampling interval is $T_s = 25\,\mu$s. Extending the prediction horizon from one to 20 steps

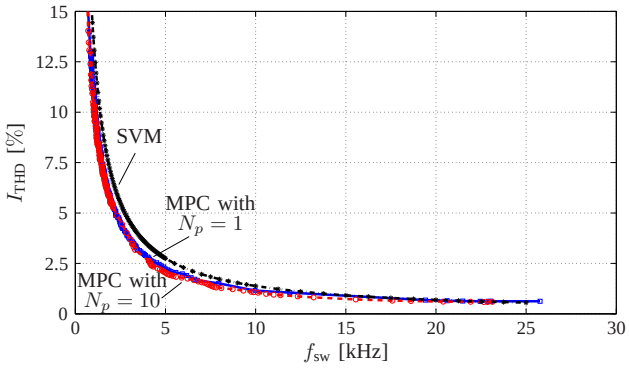

(a) I_{THD} vs f_{sw}

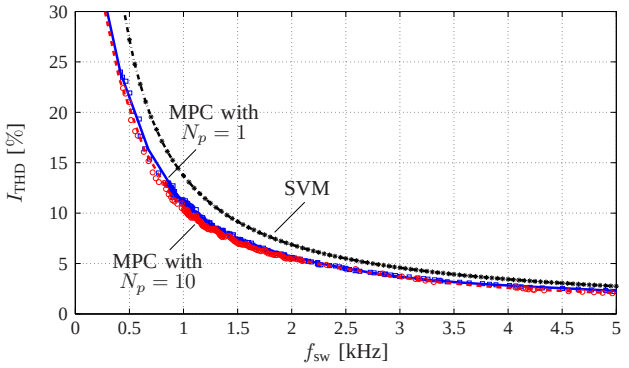

(b) I_{THD} vs f_{sw} (zoomed in)

Fig. 8: First-order (two-level drive) system: trade-off between current THD I_{THD} and switching frequency f_{sw} for FCS-MPC with $N_p = 1$ (solid, blue line), FCS-MPC with $N_p = 10$ (dashed, red line), and SVM (dash-dotted, black line). The individual simulations are shown as squares (MPC with $N_p = 1$), circles (MPC with $N_p = 10$), and asterisks (SVM).

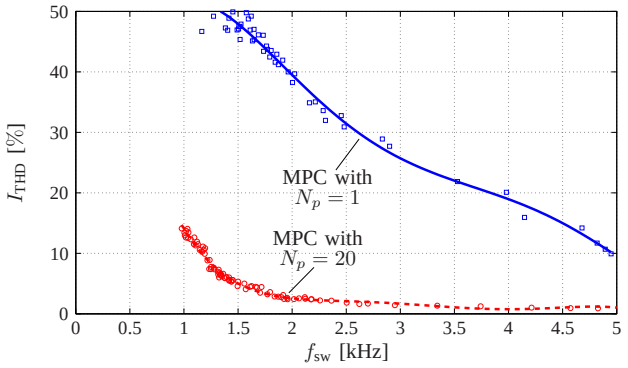

Fig. 9: Third-order (two-level inverter with an LC filter and IM) system: trade-off between stator current THD I_{THD} and switching frequency f_{sw} for FCS-MPC with $N_p = 1$ (solid, blue line), and FCS-MPC with $N_p = 20$ (dashed, red line). The individual simulations are shown as squares (MPC with $N_p = 1$), and circles (MPC with $N_p = 20$).

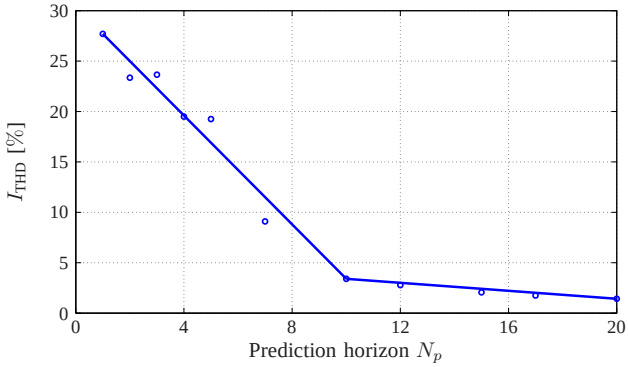

Fig. 10: Stator current THD I_{THD} of a third-order drive system as a function of the prediction horizon N_p at a switching frequency of $f_{\text{sw}} \approx 3\,\text{kHz}$. Individual simulations are shown as circles.

reduces the stator current THD by more than 75% over the whole range of the depicted switching frequencies.

This can also be observed in Fig. 10, which depicts the stator current THD as a function of the prediction horizon length for the fixed switching frequency of $3\,\text{kHz}$. The current THD decreases considerably up to the 10-step horizon, after which the rate is significantly lower. The proverbial *knee* of the fitted curve indicates a good compromise between performance and controller complexity. For the specific case study, ten-step FCS-MPC provides a good performance at a relatively low computational complexity.

Design guideline 7. *For higher-order systems, long horizons offer significant performance benefits over one-step FCS-MPC. Even a relatively short prediction horizon can considerably improve the performance, and should, thus, be adopted.*

VII. Suboptimal MPC

To facilitate the implementation of FCS-MPC algorithms, researchers resort to strategies that simplify the optimization problem at hand by either reformulating the objective function, or by restricting the feasible set[7] [24], [38], [75], [88]–[92]. However, there are cases where such methods—often unknowingly—have a detrimental effect on the system performance because they impact optimality. This section focuses on such methods and discusses the introduced suboptimality.

A. Simplified Objective Function

As discussed in Section IV, problem (10) is a multi-criterion optimization problem with multiple terms in the objective function. Weighting factors are required to set their relative importance in the objective function [58]. To avoid the tuning procedure, a simplified FCS-MPC approach is to consider multiple objective functions, each with a single term. Subsequently, the single-objective functions are minimized separately one after another, i.e., in a *sequential manner*, see, e.g., [93], [94]. Eliminating the weighting factors in such a way, nevertheless, removes degrees of freedom that can be exploited to improve the performance. This will be explained with the following example.

Example 1. *Consider one-step FCS-MPC to control the torque T_e and stator flux magnitude Ψ_s of an induction machine. By neglecting the control effort term, objective function* (8) *simplifies to*

$$J\big(\boldsymbol{x}(k), \boldsymbol{u}(k)\big) = \lambda_T J_T + (1 - \lambda_T) J_\Psi \,, \qquad (17)$$

[7] A feasible set is a set of all feasible points of an optimization problem [58, Section 4.1]. In the context of FCS-MPC for power electronics, feasible points are the switch positions $\boldsymbol{u} \in \boldsymbol{\mathcal{U}}$ that meet the constraints in (10).

where

$$J_T = \big(T_{e,ref}(k+1) - T_e(k+1)\big)^2, \tag{18a}$$

$$J_\Psi = \big(\Psi_{s,ref}(k+1) - \Psi_s(k+1)\big)^2, \tag{18b}$$

and $\lambda_T \in [0,1]$. *As shown in [22],* J_T *can be written as*

$$J_T = c_m\big(\psi^*_{sq}(k+1) - \psi_{sq}(k+1)\big)^2, \tag{19}$$

where c_m *is a machine-dependent constant parameter. We also define* $\Psi_s = \|\boldsymbol{\psi}_s\|_2$.

The level sets of J_T *are straight lines parallel to the rotor flux vector* $\boldsymbol{\psi}_r$, *see [22, Fig. 3(a)]. The level sets of* J_Ψ *are concentric circles centered at the origin of the Cartesian plane, see [22, Fig. 3(b)]. This implies that the two level sets are not orthogonal to each other, and that the minimization of the two terms in the objective function is coupled.*

As discussed in Section III-B, λ_T *can be chosen algebraically so as to combine the aforementioned level sets of the individual terms in a way that achieves a favorable system performance, see [49, Section V]. In doing so, both terms can be simultaneously minimized in an optimal manner.*

In [93], however, it is proposed to split the objective function (17) *into its two terms* J_T *and* J_Ψ, *and to minimize them sequentially so as to avoid the tuning procedure. In a first step, two three-phase switch positions are computed that achieve the lowest value of* J_T *in* (18a). *In a second step, the switch position that minimizes* J_Ψ *in* (18b) *is determined and applied to the converter. When doing so, only the previously computed two switch positions are considered*[8].

This turns the two-dimensional MPC problem with objective function (17) *into a sequence of two one-dimensional problems; the flux vector is first controlled along the* q*-axis, and, following, along the* d*-axis. As can be understood, this limits the controllability of the torque and machine magnetization and can thus lead to suboptimal performance.*

The suboptimality of this method is verified in Fig. 11 for the two-level drive system in Appendix A. The optimal flux/torque FCS-MPC discussed in Section III-B is compared with the aforementioned suboptimal approach. As can be seen, when the torque and flux terms are minimized sequentially significantly higher current distortions result over the whole range of switching frequencies. Note that since the sequential approach does not consider a control effort term, the switching frequency is varied by changing the sampling interval T_s.

Design guideline 8. *The weighting factors in multi-criterion MPC add degrees of freedom that ensure operation at the optimal trade-off surface, and are thus vital. By adjusting these weights, i.e., by assigning different priorities among the objective function terms, all objectives can be simultaneously met and optimality is guaranteed.*

B. Direct Rounding

The straightforward method to keep the computational cost of the optimization process to a minimum is to round

[8]This method can be extended to different objectives, sequence of objective functions, and numbers of options to be evaluated, see e.g., [94].

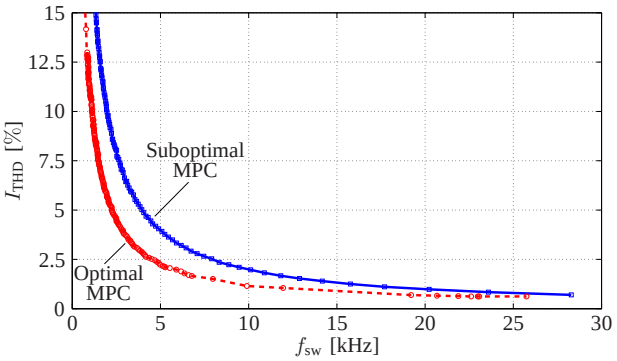

Fig. 11: Trade-off between current THD I_{THD} and switching frequency f_{sw} for suboptimal (solid, blue line), and optimal (dashed, red line) torque/flux FCS-MPC. The individual simulations are shown as squares (suboptimal FCS-MPC), and circles (optimal FCS-MPC).

(i.e., quantize) the unconstrained solution $\boldsymbol{u}_{\mathrm{unc}}(k)$ (see Section IV-A). This means that the entries of $\boldsymbol{u}_{\mathrm{unc}}(k)$ are rounded componentwise to the nearest integer of $\mathcal{U}$, see, e.g., [86], [95]. Hence, the applied switch position $\boldsymbol{u}_{\mathrm{rnd}}(k)$ is

$$\boldsymbol{u}_{\mathrm{rnd}}(k) = \lceil \boldsymbol{u}_{\mathrm{unc}}(k) \rfloor. \tag{20}$$

By doing so, however, suboptimal solutions are occasionally implemented because the optimal and quantized solutions do not always coincide, i.e., $\boldsymbol{u}^*(k) \neq \boldsymbol{u}_{\mathrm{rnd}}(k)$. This will be exemplified in the following example.

Example 2. *Consider a two-level converter system of the form* (3) *and FCS-MPC* (10) *with* $N_p = 1$. *Assume that at some instance of the problem the unconstrained solution is*

$$\boldsymbol{u}_{unc}(k) = \begin{bmatrix} 0.2416 & -0.3401 & 0.0985 \end{bmatrix}^T.$$

This is depicted in Fig. 12(a) in the ab*-plane*[9] *along with possible integer solutions. Rounding the unconstrained solution* $\boldsymbol{u}_{rnd}$ *yields*

$$\boldsymbol{u}_{rnd}(k) = \begin{bmatrix} 1 & -1 & 1 \end{bmatrix}^T,$$

which is also shown in Fig. 12(a). To examine whether the quantized unconstrained solution is the solution to the optimization problem (10) *it is recommended to revisit the problem and examine it from a different perspective. As shown in [24], function* (8) *can be written as*

$$J\big(\boldsymbol{x}(k), \boldsymbol{u}(k)\big) = \|\boldsymbol{V}\boldsymbol{u}_{unc}(k) - \boldsymbol{V}\boldsymbol{u}(k)\|_2^2, \tag{21}$$

where the so-called generator matrix $\boldsymbol{V}$ *generates the (truncated) lattice*

$$\mathcal{L}(\boldsymbol{V}) = \left\{ \sum_{i=1}^{3} w_i \boldsymbol{v}_i \mid w_i \in \{-1, 1\} \right\}.$$

Minimizing (21) *can be interpreted as finding the three-phase switch position* $\boldsymbol{u}$ *(i.e., lattice point) closest (in the Euclidean sense) to the unconstrained solution* $\boldsymbol{u}_{unc}$. *Assuming*

$$\boldsymbol{V} = \begin{bmatrix} 14.45 & 0 & 0 \\ -7.07 & 15.95 & 0 \\ -0.09 & -0.09 & 16.32 \end{bmatrix} \cdot 10^{-3},$$

[9]The c-axis is not depicted to simplify the visualization.

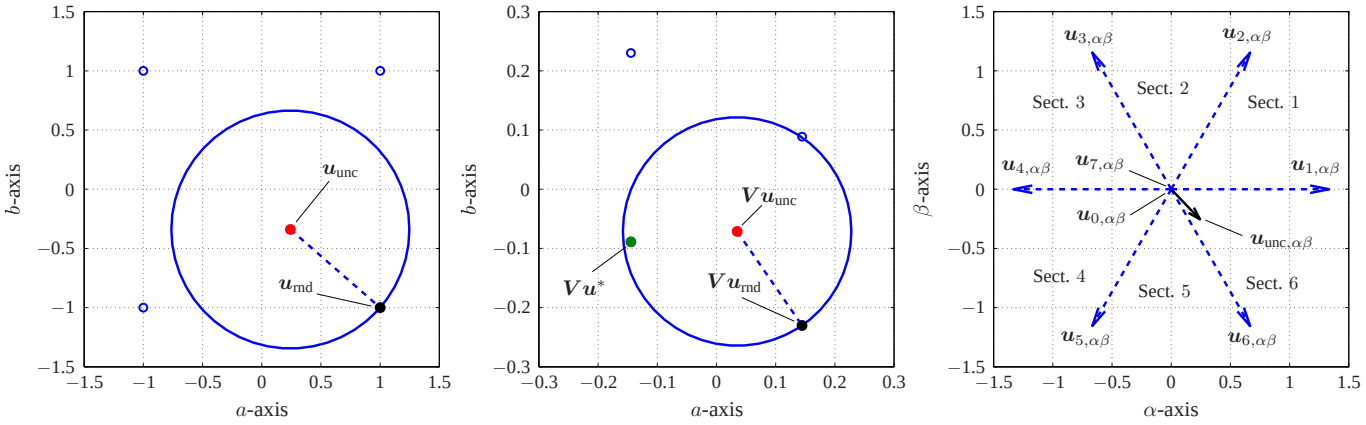

(a) Original ab-plane.

(b) Transformed ab-plane as created by the generator matrix $\boldsymbol{V}$.

(c) $\alpha\beta$-plane.

Fig. 12: Visualization of the FCS-MPC problem with $N_p = 1$ in the (a) original ab-plane (the c-axis is not shown), (b) ab-plane transformed by the generator matrix $\boldsymbol{V}$, and (c) $\alpha\beta$-plane, assuming a two-level converter. In (a) and (b), the unconstrained solution is shown as the solid red circle, the rounded solution as the black solid circle, the optimal solution as the green solid circle, and the remaining integer candidate solutions (i.e., the three-phase switch positions $\boldsymbol{u}_i$, $i \in \{0, 1, \dots 7\}$) as circles.

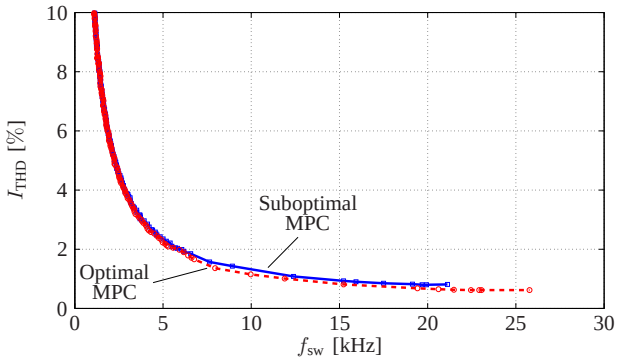

Fig. 13: Trade-off between current THD I_{THD} and switching frequency f_{sw} for suboptimal MPC via direct rounding (solid, blue line), and optimal FCS-MPC (dashed, red line). The individual simulations are shown as squares (suboptimal MPC), and circles (optimal MPC).

the transformed abc-plane becomes skewed, as illustrated in Fig. 12(b) for the a- and b-axes. Because of this transformation $\boldsymbol{u}_{rnd}$ turns out to be not *the lattice point closest to $\boldsymbol{u}_{unc}$. Indeed, minimizing* (21) *yields*

$$\boldsymbol{u}^*(k) = \begin{bmatrix} -1 & -1 & 1 \end{bmatrix}^T$$

as the solution to the optimization problem, which is the point closest to $\boldsymbol{u}_{unc}$. This fact can also be observed in Fig. 12(b).

Thus, direct rounding can lead to a suboptimal performance. This is confirmed by Fig. 13, which considers one-step FCS-MPC for the drive system case study in Appendix A with the sampling interval $T_s = 5\,\mu$s. We conclude that the integer solution needs to be found with a method that guarantees optimality, such as exhaustive enumeration or a dedicated branch-and-bound method, see, e.g., the sphere decoder [24].

Design guideline 9. *Direct quantization of the unconstrained solution incurs a degree of suboptimality. Therefore, it should not be used in lieu of more sophisticated algorithms that guarantee optimality.*

C. Restricted Feasible Set

Due to the pronounced computational cost of FCS-MPC algorithms, methods to reduce the computational complexity of (10) attract the research interest [24], [38], [88], [90]–[92]. A common approach is to limit the search space, i.e., to reduce the number of candidate solutions to be considered. To this end, the unconstrained solution $\boldsymbol{u}_{\text{unc}}$ to (10)—see (12)—is most frequently utilized along with methods, such as branch-and-bound algorithms, or heuristics to speed up the optimization process [96]. However, there are cases where the adopted heuristics unintentionally exclude the optimal solution $\boldsymbol{u}^*$ from the feasible set. As a result, a degree of suboptimality is introduced that leads to performance deterioration.

A popular approach is to restrict the feasible set to that triangular sector of the $\alpha\beta$-plane wherein the unconstrained solution lies [38], [40], [68], [90], [92], [97]–[99]. Assuming a three-phase two-level inverter, the seven unique vectors form six triangular sectors, as can be seen in Fig. 12(c); depending on the location of the unconstrained vector $\boldsymbol{u}_{\text{unc},\alpha\beta} = \boldsymbol{K}(0)\boldsymbol{u}_{\text{unc}}$, the corresponding sector and the three vectors that form it are identified.

This heuristic method greatly reduces the size of the feasible set. Returning to the example of the two-level inverter, the number of candidate switch positions is reduced from 7^{N_p} to 3^{N_p}. This difference—and the reduction of the computational burden—becomes more evident as the number of the switching devices of the converter increases. However, the above-mentioned technique comes with a pitfall, because it is also prone to suboptimality. This is explained with the following example.

Example 3. *Consider the same setup and conditions as in Example 2. Transforming $\boldsymbol{u}_{unc} = [0.2416 \;\; -0.3401 \;\; 0.0985]^T$ into the $\alpha\beta$-plane gives*

$$\boldsymbol{u}_{unc,\alpha\beta}(k) = \boldsymbol{K}(0)\boldsymbol{u}_{unc}(k) = \begin{bmatrix} 0.2416 & -0.2532 \end{bmatrix}^T .$$

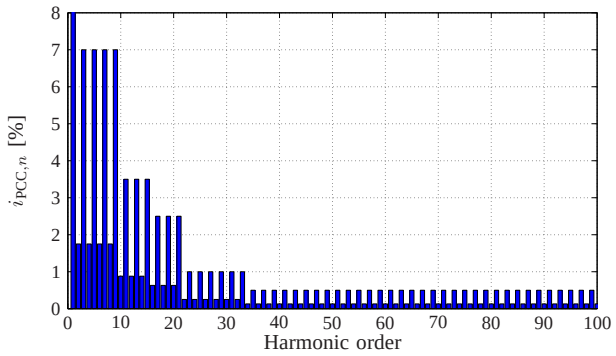

Fig. 14: Current harmonic limits at the PCC based on the IEEE 519 standard for a short-circuit ratio of $k_{\mathrm{sc}} = 20$.

As shown in Fig. 12(c), $\boldsymbol{u}_{unc,\alpha\beta}$ is located within Sector 6, thus the vectors

$$\begin{aligned}\boldsymbol{u}_{0,\alpha\beta} &= \boldsymbol{K}(0)[-1\ -1\ -1]^T\,,\\ \boldsymbol{u}_{1,\alpha\beta} &= \boldsymbol{K}(0)[1\ -1\ -1]^T\,,\\ \boldsymbol{u}_{6,\alpha\beta} &= \boldsymbol{K}(0)[1\ -1\ 1]^T\,,\ \textit{and}\\ \boldsymbol{u}_{7,\alpha\beta} &= \boldsymbol{K}(0)[1\ 1\ 1]^T\end{aligned}$$

are the vectors (switch positions) to be evaluated. Note that $\boldsymbol{u}_{rnd}$ is among the candidate solutions.

However, as shown in Example 2, the optimal solution is $\boldsymbol{u}^*(k) = [-1\ -1\ 1]^T$. This switch position was excluded from the restricted feasible set, hence a suboptimal switch position is to be applied to the converter.

Design guideline 10. *Restrictions on the feasible set of the considered switch positions have to be implemented with caution and only after careful analysis of the problem at hand. Otherwise, FCS-MPC may deliver suboptimal results that will affect the system performance accordingly.*

VIII. Performance Assessment

FCS-MPC performs the control and modulation tasks in one computational stage, see Fig. 3. Consequently, a subsequent modulation stage is not required. The lack thereof and the FCS-MPC problem formulation (10) not imposing a periodic switching pattern imply non-deterministic harmonic spectra. This is usually not an issue for inverters driving electrical machines; for drives, the current THD is the main performance metric because it relates to the harmonic machine losses.

For grid-connected converters, however, FCS-MPC in the form (10) is not suitable. The reason is that such applications have to meet grid codes that limit the amplitudes of the voltage and current harmonics injected at the point of common coupling (PCC). One widely imposed grid code is the IEEE 519 standard [100], which imposes particularly stringent limits on even harmonics, see Fig. 14.

The absence of a modulator also implies a variable switching frequency. This complicates the system design and might lead to an overly conservative choice for the output filter, cooling system, and semiconductor devices. Therefore, there is a need to ensure a constant, or at least deterministic, switching frequency. In this direction, ongoing research aims to extend the problem formulation (10) of standard FCS-MPC, see, e.g., [63]–[67], [69]–[71], [101]–[104]; see also the discussion in Section IV-C.

The literature on FCS-MPC mostly considers two-level converters operating in the kHz range [8], [27], [41], [45], [47], [48], [53], [81], [82], [105], [106]. At such high switching frequencies, the benefit of FCS-MPC over established modulator-based methods (such as SVM) remains unclear. This observation is also highlighted in Fig. 7 and Table II; a very small sampling interval T_s is required to outperform SVM at relatively high switching frequencies. Hence, such a small T_s, combined with the—generally demanding and complicated—enumeration strategy, poses an implementation challenge.

Given the above pitfalls and challenges of FCS-MPC, one remedy is to consider indirect MPC, which uses a modulator and offers several advantages. First, the power converter is operated at a constant switching frequency. Moreover, deterministic harmonic spectra result. The harmonic components are limited to non-triplen odd integer multiples of the fundamental frequency, provided that the carrier frequency is three times an odd integer multiple of the fundamental frequency. Finally, the optimization problem underlying indirect MPC can be cast as a QP, which is computationally relatively straightforward to solve [58] in real time with existing solvers, see, e.g., [19], [107]–[109]. This research direction is steadily gaining attention [110]–[112]. If constraints on state variables can be neglected, the linear quadratic regulator (LQR) might prove an interesting alternative [113], [114].

Design guideline 11. *FCS-MPC in its current form is not suitable for grid-connected converters and when operating at high switching frequencies.*

IX. Conclusions

FCS-MPC is a promising and versatile predictive control method. It is particularly suitable for complex power electronic systems operating at their physical limits. However, commonly used design simplifications limit its performance potential in terms of current distortions per switching frequency; this prohibits the adoption of FCS-MPC by industry. The main factors that affect the performance of FCS-MPC were analyzed and discussed in this paper, including the weighting factors, the sampling interval, and the length of the prediction horizon.

Several common misconceptions about FCS-MPC were identified, clarified and discussed. A number of design guidelines were provided. When following them and carefully designing FCS-MPC algorithms, significant performance benefits can be attained. These benefits were demonstrated with the first-order and third-order drive system case studies, which are based on a two-level inverter and an induction machine.

Appendix A
Case Study A: Drive System

Fig. 15 shows a two-level three-phase voltage source inverter with an induction machine. Its corresponding system parameters are summarized in Table III. The three-phase switch position $\boldsymbol{u}$ is restricted to the set $\boldsymbol{\mathcal{U}} = \{-1, 1\}^3$. Using the

TABLE III: Rated values and parameters of the drive system

Rated values		Parameters	
Induction Motor			
Voltage	400 V	Stator resistance (R_s)	2.7 Ω (0.0514 p.u.)
Current	4.4 A	Rotor resistance (R_r)	2.4 Ω (0.0457 p.u.)
Apparent power	3.048 kVA	Stator leakage reactance (X_{ls})	9.868 mH (0.0591 p.u.)
Stator frequency	50 Hz	Rotor leakage reactance (X_{lr})	11.777 mH (0.0705 p.u.)
Rotational speed	2875 rpm	Mutual reactance (X_m)	394.704 mH (2.3625 p.u.)
Inverter			
		Dc-link voltage (V_{dc})	650 V (1.9902 p.u.)
LC filter			
		Converter-side resistance (R_l)	0.54 mΩ ($0.0103 \cdot 10^{-3}$ p.u.)
		Converter-side reactance (X_l)	1.3 mH (0.0078 p.u.)
		Capacitance resistance (R_c)	0.67 mΩ ($0.0127 \cdot 10^{-3}$ p.u.)
		Capacitance reactance (X_c)	30 μF (0.4947 p.u.)

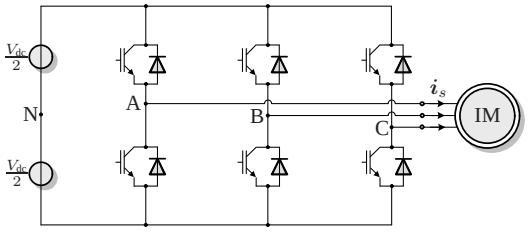

Fig. 15: Two-level inverter driving an induction machine.

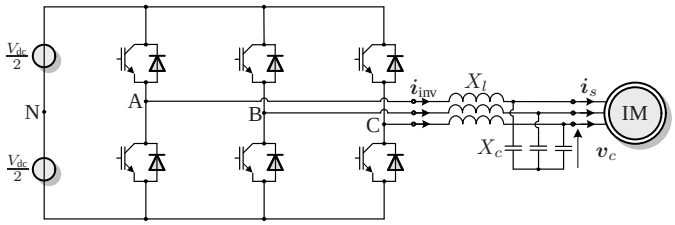

Fig. 16: Two-level inverter with an output LC filter driving an induction motor.

stator current $\boldsymbol{i}_{s,\alpha\beta}$ and the rotor flux $\boldsymbol{\psi}_{r,\alpha\beta}$ in the $\alpha\beta$-plane as the state vector, we define $\boldsymbol{x} = [i_{s\alpha}\ i_{s\beta}\ \psi_{r\alpha}\ \psi_{r\beta}]^T \in \mathbb{R}^4$. The stator current is the system output, which we set to $\boldsymbol{y} = \boldsymbol{i}_{s,\alpha\beta} \in \mathbb{R}^2$.

The corresponding continuous-time dynamical model can be easily derived; see, e.g., [14, Appendix 5.A]. Using exact Euler discretization, the linear state-space model (1) results. For this case study, the system dimensions are given by $n_u = 3$, $n_x = 4$, and $n_y = 2$, according to the notation introduced in Section II-A. Throughout this paper, the drive is operated at nominal speed and rated torque.

Appendix B
Case Study B: Drive System with an LC Filter

The drive system with the LC filter is depicted in Fig. 16, and its parameters are given in Table III. As with the previous case study presented in Appendix A, the three-phase switch position $\boldsymbol{u} \in \{-1, 1\}^3$ is the manipulated variable. The state vector consists of the inverter current $\boldsymbol{i}_{\text{inv},\alpha\beta}$, capacitor voltage $\boldsymbol{v}_{c,\alpha\beta}$, stator current $\boldsymbol{i}_{s,\alpha\beta}$, and rotor flux $\boldsymbol{\psi}_{r,\alpha\beta}$; we write $\boldsymbol{x} = [\boldsymbol{i}^T_{\text{inv},\alpha\beta}\ \boldsymbol{v}^T_{c,\alpha\beta}\ \boldsymbol{i}^T_{s,\alpha\beta}\ \boldsymbol{\psi}^T_{r,\alpha\beta}]^T \in \mathbb{R}^8$. The first six state variables are the controlled variables, i.e., $\boldsymbol{y} = [\boldsymbol{i}^T_{\text{inv},\alpha\beta}\ \boldsymbol{v}^T_{c,\alpha\beta}\ \boldsymbol{i}^T_{s,\alpha\beta}]^T \in \mathbb{R}^6$.

For a detailed derivation of the continuous-time state-space model of the system, the reader is referred to [14, Appendix 6.A]. Note that this case study is a third-order system in each coordinate axis of the $\alpha\beta$-plane. The system dimensions are $n_u = 3$, $n_x = 8$, and $n_y = 6$. The drive is operated at nominal speed and rated torque.

The combination of the LC filter with the total leakage reactance X_σ of the machine gives rise to an LCL filter structure. Neglecting the (small) ohmic resistances in the filter and stator, the resonance frequency

$$f_{\text{res}} = f_B \frac{1}{\sqrt{X_c \frac{X_l X_\sigma}{X_l + X_\sigma}}} \approx 830 \text{ Hz}\,, \tag{22}$$

can be obtained, where $f_B = 50\,\text{Hz}$ is the base (rated) frequency.

Appendix C
Proof of Theorem 2

The proof of Theorem 2 is provided hereafter.

Proof. The objective of a deadbeat controller is to eliminate the output error as quickly as possible. This implies $\boldsymbol{y}_{\text{ref}}(k+1) = \boldsymbol{y}(k+1)$ for a first-order system without input constraints. Given (3), this amounts to

$$\boldsymbol{y}_{\text{ref}}(k+1) = \boldsymbol{C}\boldsymbol{x}(k+1) = \boldsymbol{C}\big(\boldsymbol{A}\boldsymbol{x}(k) + \boldsymbol{B}\boldsymbol{K}(0)\boldsymbol{u}(k)\big)\,. \tag{23}$$

Therefore, by setting $\boldsymbol{u}_{\alpha\beta}(k) = \boldsymbol{K}(0)\boldsymbol{u}(k)$, the desired control action $\boldsymbol{u}_{\text{db},\alpha\beta} \in \mathbb{R}^2$ which drives the system to its reference within one sampling interval T_s is

$$\boldsymbol{u}_{\text{db},\alpha\beta}(k) = \boldsymbol{D}^{-1}\big(\boldsymbol{y}_{\text{ref}}(k+1) - \boldsymbol{C}\boldsymbol{A}\boldsymbol{x}(k)\big)\,, \tag{24}$$

where $\boldsymbol{D}^{-1}$ is the inverse of the matrix $\boldsymbol{C}\boldsymbol{B}$, i.e.,[10]

$$\boldsymbol{D}^{-1} = \big(\boldsymbol{C}\boldsymbol{B}\big)^{-1}\,.$$

[10]Given the assumption of one-step reachability, it is implied that $n_x \leq n_u$, see [56, Section 3]. For current control of a typical one-step reachable three-phase power electronic system, e.g., a converter connected to the grid or driving an electrical machine, it holds that $n_y = n_u$.

Utilizing the assumption of a linear system, (15) can be written as [14]

$$J(\boldsymbol{x}(k), \boldsymbol{U}(k)) = \|\boldsymbol{Y}_{\text{ref}} - \boldsymbol{\Gamma}\boldsymbol{x}(k) + \boldsymbol{\Upsilon}\boldsymbol{U}(k)\|_2^2 , \qquad (25)$$

with

$$\boldsymbol{Y}_{\text{ref}}(k) = \begin{bmatrix} \boldsymbol{y}_{\text{ref}}^T(k+1) & \boldsymbol{y}_{\text{ref}}^T(k+2) & \cdots & \boldsymbol{y}_{\text{ref}}^T(k+N_p) \end{bmatrix}^T .$$

The matrices are given by

$$\boldsymbol{\Upsilon} = \begin{bmatrix} \boldsymbol{\Upsilon}_{11} & \boldsymbol{\Upsilon}_{12} \\ \boldsymbol{\Upsilon}_{21} & \boldsymbol{\Upsilon}_{22} \end{bmatrix} = \left[\begin{array}{c|ccc} \boldsymbol{CB} & \boldsymbol{0} & \cdots & \boldsymbol{0} \\ \hline \boldsymbol{CAB} & \boldsymbol{CB} & \cdots & \boldsymbol{0} \\ \vdots & \vdots & & \vdots \\ \boldsymbol{CA}^{N_p-1}\boldsymbol{B} & \boldsymbol{CA}^{N_p-2}\boldsymbol{B} & \cdots & \boldsymbol{CB} \end{array}\right] \qquad (26)$$

and

$$\boldsymbol{\Gamma} = \begin{bmatrix} \boldsymbol{\Gamma}_1 \\ \boldsymbol{\Gamma}_2 \end{bmatrix} = \begin{bmatrix} \boldsymbol{CA} \\ \hline \boldsymbol{CA}^2 \\ \vdots \\ \boldsymbol{CA}^{N_p} \end{bmatrix} , \qquad (27)$$

where $\boldsymbol{0}$ denotes zero matrices of appropriate dimensions. The sequence of manipulated variables is defined in the $\alpha\beta$-plane as

$$\boldsymbol{U}(k) = \begin{bmatrix} \boldsymbol{u}_{\alpha\beta}^T(k) & \boldsymbol{u}_{\alpha\beta}^T(k+1) & \cdots & \boldsymbol{u}_{\alpha\beta}^T(k+N_p-1) \end{bmatrix}^T .$$

The solution $\boldsymbol{u}_{\text{unc},\alpha\beta}(k)$ of long-horizon FCS-MPC can be found by utilizing (13). Given that for $\boldsymbol{M} = \boldsymbol{M}^T \in \mathbb{R}^{n\times n}$, $\boldsymbol{c}, \boldsymbol{\xi} \in \mathbb{R}^n$, and $d \in \mathbb{R}$ it holds that

$$\nabla \left(\boldsymbol{c}^T\boldsymbol{\xi} + d\right)(\boldsymbol{\xi}) = \boldsymbol{c}$$
$$\nabla \left(\boldsymbol{\xi}^T\boldsymbol{M}\boldsymbol{\xi}\right)(\boldsymbol{\xi}) = 2\boldsymbol{M}\boldsymbol{\xi} ,$$

it follows that

$$2\boldsymbol{\Upsilon}^T\left(\boldsymbol{\Upsilon}\boldsymbol{U}_{\text{unc}}(k) + \boldsymbol{\Gamma}\boldsymbol{x}(k) - \boldsymbol{Y}_{\text{ref}}(k)\right) = \boldsymbol{0} ,$$

which implies that

$$\boldsymbol{U}_{\text{unc}}(k) = \boldsymbol{\Upsilon}^{-1}\left(\boldsymbol{Y}_{\text{ref}}(k) - \boldsymbol{\Gamma}\boldsymbol{x}(k)\right) . \qquad (28)$$

Because the problem formulation is in the $\alpha\beta$-plane it is implied that matrix $\boldsymbol{\Upsilon}_{22}$ is nonsingular. Provided that $\boldsymbol{\Upsilon}_{11} - \boldsymbol{\Upsilon}_{12}\boldsymbol{\Upsilon}_{22}^{-1}\boldsymbol{\Upsilon}_{21}$ is also nonsingular, and by utilizing the Woodbury matrix identity and (26), matrix $\boldsymbol{W} = \boldsymbol{\Upsilon}^{-1}$ can be written as

$$\boldsymbol{W} = \begin{bmatrix} \boldsymbol{W}_{11} & \boldsymbol{W}_{12} \\ \boldsymbol{W}_{21} & \boldsymbol{W}_{22} \end{bmatrix} \qquad (29)$$

with

$$\boldsymbol{W}_{11} = (\boldsymbol{\Upsilon}_{11} - \boldsymbol{\Upsilon}_{12}\boldsymbol{\Upsilon}_{22}^{-1}\boldsymbol{\Upsilon}_{21})^{-1} = \boldsymbol{\Upsilon}_{11}^{-1}$$
$$\boldsymbol{W}_{12} = -\boldsymbol{W}_{11}\boldsymbol{\Upsilon}_{12}\boldsymbol{\Upsilon}_{22}^{-1} = \boldsymbol{0}$$
$$\boldsymbol{W}_{21} = -\boldsymbol{\Upsilon}_{22}^{-1}\boldsymbol{\Upsilon}_{21}\boldsymbol{W}_{11} = -\boldsymbol{\Upsilon}_{22}^{-1}\boldsymbol{\Upsilon}_{21}\boldsymbol{\Upsilon}_{11}^{-1}$$
$$\boldsymbol{W}_{22} = \boldsymbol{\Upsilon}_{22}^{-1} + \boldsymbol{\Upsilon}_{22}^{-1}\boldsymbol{\Upsilon}_{21}\boldsymbol{W}_{11}\boldsymbol{\Upsilon}_{12}\boldsymbol{\Upsilon}_{22}^{-1} = \boldsymbol{\Upsilon}_{22}^{-1} .$$

Using (27), and (29), the unconstrained solution becomes

$$\begin{aligned} \boldsymbol{U}_{\text{unc}}(k) &= \begin{bmatrix} \boldsymbol{u}_{\text{unc},\alpha\beta}(k) \\ \hline \boldsymbol{u}_{\text{unc},\alpha\beta}(k+1) \\ \vdots \\ \boldsymbol{u}_{\text{unc},\alpha\beta}(k+N_p-1) \end{bmatrix} \\ &\overset{(28)}{=} \boldsymbol{\Upsilon}^{-1}\left[\begin{bmatrix} \boldsymbol{y}_{\text{ref}}(k+1) \\ \boldsymbol{y}_{\text{ref}}(k+2) \\ \vdots \\ \boldsymbol{y}_{\text{ref}}(k+N_p) \end{bmatrix} - \begin{bmatrix} \boldsymbol{\Gamma}_1\boldsymbol{x}(k) \\ \boldsymbol{\Gamma}_2\boldsymbol{x}(k) \end{bmatrix}\right] = \boldsymbol{\Upsilon}^{-1}\begin{bmatrix} \boldsymbol{\gamma}_1 \\ \boldsymbol{\gamma}_2 \end{bmatrix} \\ &\overset{(29)}{=} \begin{bmatrix} \boldsymbol{W}_{11} & \boldsymbol{W}_{12} \\ \boldsymbol{W}_{21} & \boldsymbol{W}_{22} \end{bmatrix}\begin{bmatrix} \boldsymbol{\gamma}_1 \\ \boldsymbol{\gamma}_2 \end{bmatrix} = \begin{bmatrix} \boldsymbol{W}_{11}\boldsymbol{\gamma}_1 + \boldsymbol{W}_{12}\boldsymbol{\gamma}_2 \\ \boldsymbol{W}_{21}\boldsymbol{\gamma}_1 + \boldsymbol{W}_{22}\boldsymbol{\gamma}_2 \end{bmatrix} \\ &= \begin{bmatrix} \boldsymbol{\Upsilon}_{11}^{-1}\boldsymbol{\gamma}_1 \\ -\boldsymbol{\Upsilon}_{22}^{-1}\boldsymbol{\Upsilon}_{21}\boldsymbol{W}_{11}\boldsymbol{\gamma}_1 + \boldsymbol{\Upsilon}_{22}^{-1}\boldsymbol{\gamma}_2 \end{bmatrix} . \end{aligned}$$

According to the receding horizon policy, only the control action that refers to time step k is implemented. Thus, by considering (26), it follows that

$$\boldsymbol{u}_{\text{unc},\alpha\beta}(k) = \boldsymbol{D}^{-1}\left(\boldsymbol{y}_{\text{ref}}(k+1) - \boldsymbol{CAx}(k)\right) . \qquad (30)$$

As can be observed from (24) and (30), the deadbeat solution is the same as the first element of the relaxed solution of FCS-MPC with objective function (15).

■

ACKNOWLEDGMENT

The authors would like to thank Pablo Acuña, Sergio Vazquez, Marco Rivera, Fengxiang Wang, Pablo Lezana, and Margarita Norambuena for their valuable feedback.

REFERENCES

[1] J. B. Rawlings and D. Q. Mayne, *Model predictive control: Theory and design.* Madison, WI: Nob Hill, 2009.

[2] S. J. Qin and T. A. Badgwell, "A survey of industrial model predictive control technology," *Control Eng. Pract.*, vol. 11, pp. 733–764, Jul. 2003.

[3] J. Holtz and S. Stadtfeld, "A predictive controller for the stator current vector of ac-machines fed from a switched voltage source," in *Int. Power Electron. Conf.*, vol. 2, (Tokyo, Japan), pp. 1665–1675, Mar. 1983.

[4] D. F. Schröder and R. Kennel, "Model-control PROMC—A new control strategy with microcomputer for drive applications," *IEEE Trans. Ind. Appl.*, vol. IA-21, pp. 1162–1167, Sep./Oct. 1985.

[5] A. Linder and R. Kennel, "Model predictive control for electrical drives," in *Proc. IEEE Power Electron. Spec. Conf.*, (Recife, Brazil), pp. 1793–1799, Jun. 2005.

[6] T. Geyer, G. Papafotiou, and M. Morari, "On the optimal control of switch-mode dc-dc converters," in *Hybrid Syst.: Comput. and Control* (R. Alur and G. J. Pappas, eds.), vol. 2993 of *LNCS*, pp. 342–356, Berlin, Germany: Springer-Verlag, 2004.

[7] T. Geyer, *Low complexity model predictive control in power electronics and power systems*. PhD thesis, Autom. Control Lab. ETH Zurich, Zurich, Switzerland, 2005.

[8] J. Rodríguez, J. Pontt, C. A. Silva, P. Correa, P. Lezana, P. Cortés, and U. Ammann, "Predictive current control of a voltage source inverter," *IEEE Trans. Ind. Electron.*, vol. 54, pp. 495–503, Feb. 2007.

[9] P. Cortés, M. P. Kazmierkowski, R. M. Kennel, D. E. Quevedo, and J. Rodríguez, "Predictive control in power electronics and drives," *IEEE Trans. Ind. Electron.*, vol. 55, pp. 4312–4324, Dec. 2008.

[10] J. Rodríguez, M. P. Kazmierkowski, J. R. Espinoza, P. Zanchetta, H. Abu-Rub, H. A. Young, and C. A. Rojas, "State of the art of finite control set model predictive control in power electronics," *IEEE Trans. Ind. Informat.*, vol. 9, pp. 1003–1016, May 2013.

[11] S. Kouro, M. A. Perez, J. Rodríguez, A. M. Llor, and H. A. Young, "Model predictive control: MPC's role in the evolution of power electronics," *IEEE Ind. Electron. Mag.*, vol. 9, pp. 8–21, Dec. 2015.

[12] S. Vazquez, J. Rodríguez, M. Rivera, L. G. Franquelo, and M. Norambuena, "Model predictive control for power converters and drives: Advances and trends," *IEEE Trans. Ind. Electron.*, vol. 64, pp. 935–947, Feb. 2017.

[13] J. Rodríguez and P. Cortés, *Predictive control of power converters and electrical drives*. Chichester, UK: Wiley, 2012.

[14] T. Geyer, *Model predictive control of high power converters and industrial drives*. Hoboken, NJ: Wiley, 2016.

[15] G. A. Papafotiou, G. D. Demetriades, and V. G. Agelidis, "Technology readiness assessment of model predictive control in medium- and high-voltage power electronics," *IEEE Trans. Ind. Electron.*, vol. 63, pp. 5807–5815, Sep. 2016.

[16] T. Geyer, N. Oikonomou, G. Papafotiou, and F. D. Kieferndorf, "Model predictive pulse pattern control," *IEEE Trans. Ind. Appl.*, vol. 48, pp. 663–676, Mar./Apr. 2012.

[17] N. Oikonomou, C. Gutscher, P. Karamanakos, F. D. Kieferndorf, and T. Geyer, "Model predictive pulse pattern control for the five-level active neutral point clamped inverter," *IEEE Trans. Ind. Appl.*, vol. 49, pp. 2583–2592, Nov./Dec. 2013.

[18] T. J. Besselmann, S. Van de moortel, S. Almér, P. Jörg, and H. J. Ferreau, "Model predictive control in the multi-megawatt range," *IEEE Trans. Ind. Electron.*, vol. 63, pp. 4641–4648, Jul. 2016.

[19] T. J. Besselmann, S. Almér, and H. J. Ferreau, "Model predictive control of load-commutated inverter-fed synchronous machines," *IEEE Trans. Power Electron.*, vol. 31, pp. 7384–7393, Oct. 2016.

[20] M. Vasiladiotis, A. Christe, and T. Geyer, "Model predictive pulse pattern control for modular multilevel converters," *IEEE Trans. Ind. Electron.*, vol. 66, pp. 2423–2431, Mar. 2019.

[21] R. S. Palais and R. A. Palais, *Differential equations, mechanics, and computation*. Providence, RI: Amer. Mathem. Soc., 2009.

[22] T. Geyer, "Algebraic tuning guidelines for model predictive torque and flux control," *IEEE Trans. Ind. Appl.*, vol. 54, pp. 4464–4475, Sep./Oct. 2018.

[23] R. P. Aguilera and D. E. Quevedo, "Stability analysis of quadratic MPC with a discrete input alphabet," *IEEE Trans. Autom. Control*, vol. 58, pp. 3190–3196, Dec. 2013.

[24] T. Geyer and D. E. Quevedo, "Multistep finite control set model predictive control for power electronics," *IEEE Trans. Power Electron.*, vol. 29, pp. 6836–6846, Dec. 2014.

[25] P. Karamanakos, T. Geyer, N. Oikonomou, F. D. Kieferndorf, and S. Manias, "Direct model predictive control: A review of strategies that achieve long prediction intervals for power electronics," *IEEE Ind. Electron. Mag.*, vol. 8, pp. 32–43, Mar. 2014.

[26] R. Vargas, P. Cortés, U. Ammann, J. Rodríguez, and J. Pontt, "Predictive control of a three-phase neutral-point-clamped inverter," *IEEE Trans. Power Electron.*, vol. 24, pp. 2697–2705, Oct. 2007.

[27] P. Cortés, J. Rodríguez, P. Antoniewicz, and M. Kazmierkowski, "Direct power control of an AFE using predictive control," *IEEE Trans. Power Electron.*, vol. 23, pp. 2516–2523, Sep. 2008.

[28] R. Vargas, U. Ammann, and J. Rodríguez, "Predictive approach to increase efficiency and reduce switching losses on matrix converters," *IEEE Trans. Power Electron.*, vol. 24, pp. 894–902, Apr. 2009.

[29] P. Correa, J. Rodríguez, I. Lizama, and D. Andler, "A predictive control scheme for current-source rectifiers," *IEEE Trans. Ind. Electron.*, vol. 56, pp. 1813–1815, May 2009.

[30] R. Vargas, U. Ammann, B. Hudoffsky, J. Rodríguez, and P. W. Wheeler, "Predictive torque control of an induction machine fed by a matrix converter with reactive input power control," *IEEE Trans. Power Electron.*, vol. 25, pp. 1426–1438, Jun. 2010.

[31] M. Rivera, C. Rojas, J. Rodríguez, P. Wheeler, B. Wu, and J. Espinoza, "Predictive current control with input filter resonance mitigation for a direct matrix converter," *IEEE Trans. Power Electron.*, vol. 26, pp. 2794–2803, Oct. 2011.

[32] J. Qin and M. Saeedifard, "Predictive control of a modular multilevel converter for a back-to-back HVDC system," *IEEE Trans. Power Del.*, vol. 27, pp. 1538–1647, Jul. 2012.

[33] P. Karamanakos, K. Pavlou, and S. Manias, "An enumeration-based model predictive control strategy for the cascaded H-bridge multilevel rectifier," *IEEE Trans. Ind. Electron.*, vol. 61, pp. 3480–3489, Jul. 2014.

[34] Z. Zhang, F. Wang, T. Sun, J. Rodríguez, and R. Kennel, "FPGA-based experimental investigation of a quasi-centralized model predictive control for back-to-back converters," *IEEE Trans. Power Electron.*, vol. 31, pp. 662–674, Jan. 2016.

[35] K. Antoniewicz, M. Jasinski, M. P. Kazmierkowski, and M. Malinowski, "Model predictive control for three-level four-leg flying capacitor converter operating as shunt active power filter," *IEEE Trans. Ind. Electron.*, vol. 63, pp. 5255–5262, Aug. 2016.

[36] H. A. Young, M. A. Perez, and J. Rodríguez, "Analysis of finite-control-set model predictive current control with model parameter mismatch in a three-phase inverter," *IEEE Trans. Ind. Electron.*, vol. 63, pp. 3100–3107, May 2016.

[37] M. Mosa, R. S. Balog, and H. Abu-Rub, "High performance predictive control of quasi impedance source inverter," *IEEE Trans. Power Electron.*, vol. 32, pp. 3251–3262, Apr. 2017.

[38] Z. Zhang, C. M. Hackl, and R. Kennel, "Computationally efficient DMPC for three-level NPC back-to-back converters in wind turbine systems with PMSG," *IEEE Trans. Power Electron.*, vol. 32, pp. 8018–8034, Oct. 2017.

[39] M. Abdelrahem, C. M. Hackl, and R. Kennel, "Finite position set-phase locked loop for sensorless control of direct-driven permanent-magnet synchronous generators," *IEEE Trans. Power Electron.*, vol. 33, pp. 3097–3105, Apr. 2018.

[40] M. Siami, D. A. Khaburi, and J. Rodríguez, "Simplified finite control set-model predictive control for matrix converter-fed PMSM drives," *IEEE Trans. Power Electron.*, vol. 33, pp. 2438–2446, Mar. 2018.

[41] O. Sandre-Hernandez, J. Rangel-Magdaleno, and R. Morales-Caporal, "A comparison on finite-set model predictive torque control schemes for PMSMs," *IEEE Trans. Power Electron.*, vol. 33, pp. 8838–8847, Oct. 2018.

[42] P. Karamanakos, T. Geyer, and R. Kennel, "On the choice of norm in finite control set model predictive control," *IEEE Trans. Power Electron.*, vol. 33, pp. 7105–7117, Aug. 2018.

[43] R. P. Aguilera and D. E. Quevedo, "Predictive control of power converters: Designs with guaranteed performance," *IEEE Trans. Ind. Informat.*, vol. 11, pp. 53–63, Feb. 2015.

[44] A. V. Oppenheim, A. S. Willsky, and S. H. Nawab, *Signals and systems*. Upper Saddle River, NJ: Prentice-Hall, 2nd ed., 1996.

[45] D.-K. Choi and K.-B. Lee, "Dynamic performance improvement of ac/dc converter using model predictive direct power control with finite control set," *IEEE Trans. Ind. Electron.*, vol. 62, pp. 757–767, Feb. 2015.

[46] Y. Zhang, W. Xie, Z. Li, and Y. Zhang, "Model predictive direct power control of a PWM rectifier with duty cycle optimization," *IEEE Trans. Power Electron.*, vol. 28, pp. 5343–5351, Nov. 2013.

[47] H. Miranda, P. Cortés, J. I. Yuz, and J. Rodríguez, "Predictive torque control of induction machines based on state-space models," *IEEE Trans. Ind. Electron.*, vol. 56, pp. 1916–1924, Jun. 2009.

[48] J. Rodríguez, R. M. Kennel, J. R. Espinoza, M. Trincado, C. A. Silva, and C. A. Rojas, "High-performance control strategies for electrical drives: An experimental assessment," *IEEE Trans. Ind. Electron.*, vol. 59, pp. 812–820, Feb. 2012.

[49] P. Karamanakos and T. Geyer, "Model predictive torque and flux control minimizing current distortions," *IEEE Trans. Power Electron.*, vol. 34, pp. 2007–2012, Mar. 2019.

[50] K. J. Åström and B. Wittenmark, *Computer-controlled systems: Theory and design*. Upper Saddle River, NJ: Prentice-Hall, 3rd ed., 1997.

[51] T. Kawabata, T. Miyashita, and Y. Yamamoto, "Dead beat control of three phase PWM inverter," *IEEE Trans. Power Electron.*, vol. 5, pp. 21–28, Jan. 1990.

[52] L. Malesani, P. Mattavelli, and S. Buso, "Robust dead-beat current control for PWM rectifiers and active filters," *IEEE Trans. Ind. Appl.*, vol. 35, pp. 613–620, May/Jun. 1999.

[53] D. E. Quevedo, R. P. Aguilera, M. A. Pérez, P. Cortés, and R. Lizana, "Model predictive control of an AFE rectifier with dynamic references," *IEEE Trans. Power Electron.*, vol. 27, pp. 3128–3136, Jul. 2012.

[54] M. Narimani, B. Wu, V. Yaramasu, Z. Cheng, and N. R. Zargari, "Finite control-set model predictive control (FCS-MPC) of nested neutral point-clamped (NNPC) converter," *IEEE Trans. Power Electron.*, vol. 30, pp. 7262–7269, Dec. 2015.

[55] C. Zheng, T. Dragičević, and F. Blaabjerg, "Current-sensorless finite-set model predictive control for LC-filtered voltage source inverters," *IEEE Trans. Power Electron.*, vol. 35, pp. 1086–1095, Jan. 2020.

[56] D. E. Quevedo, R. P. Aguilera, and T. Geyer, "Predictive control in power electronics and drives: Basic concepts, theory and methods," in *Adv. and Intell. Control in Power Electron. and Drives* (T. Orlowska-

Kowalska, F. Blaabjerg, and J. Rodríguez, eds.), vol. 531 of *Studies in Comput. Intell.*, pp. 181–226, Springer-Verlag, 2014.
[57] J. Holtz, "Pulsewidth modulation—a survey," *IEEE Trans. Ind. Electron.*, vol. 39, pp. 410–420, Oct. 1992.
[58] S. Boyd and L. Vandenberghe, *Convex optimization*. Cambridge, UK: Cambridge Univ. Press, 2004.
[59] P. Cortés, S. Kouro, B. L. Rocca, R. Vargas, J. Rodríguez, J. I. León, S. Vazquez, and L. G. Franquelo, "Guidelines for weighting factors design in model predictive control of power converters and drives," in *Proc. IEEE Int. Conf. Ind. Technol.*, (Gippsland, Australia), pp. 1–7, Feb. 2009.
[60] S. A. Davari, D. A. Khaburi, and R. Kennel, "An improved FCS-MPC algorithm for an induction motor with an imposed optimized weighting factor," *IEEE Trans. Power Electron.*, vol. 27, pp. 1540–1551, Mar. 2012.
[61] T. Dragičević and M. Novak, "Weighting factor design in model predictive control of power electronic converters: An artificial neural network approach," *IEEE Trans. Ind. Electron.*, vol. 66, pp. 8870–8880, Nov. 2019.
[62] B. Stellato, T. Geyer, and P. J. Goulart, "High-speed finite control set model predictive control for power electronics," *IEEE Trans. Power Electron.*, vol. 32, pp. 4007–4020, May 2017.
[63] L. Tarisciotti, P. Zanchetta, A. Watson, S. Bifaretti, and J. C. Clare, "Modulated model predictive control for a seven-level cascaded H-bridge back-to-back converter," *IEEE Trans. Ind. Electron.*, vol. 61, pp. 5375–5383, Oct. 2014.
[64] S. Vazquez, A. Marquez, R. Aguilera, D. Quevedo, J. I. Leon, and L. G. Franquelo, "Predictive optimal switching sequence direct power control for grid-connected power converters," *IEEE Trans. Ind. Electron.*, vol. 62, pp. 2010–2020, Apr. 2015.
[65] M. Tomlinson, H. du T. Mouton, R. Kennel, and P. Stolze, "A fixed switching frequency scheme for finite-control-set model predictive control—Concept and algorithm," *IEEE Trans. Ind. Electron.*, vol. 63, pp. 7662–7670, Dec. 2016.
[66] S. Vazquez, R. P. Aguilera, P. Acuna, J. Pou, J. I. Leon, L. G. Franquelo, and V. G. Agelidis, "Model predictive control for single-phase NPC converters based on optimal switching sequences," *IEEE Trans. Ind. Electron.*, vol. 63, pp. 7533–7541, Dec. 2016.
[67] L. Tarisciotti, A. Formentini, A. Gaeta, M. Degano, P. Zanchetta, R. Rabbeni, and M. Pucci, "Model predictive control for shunt active filters with fixed switching frequency," *IEEE Trans. Ind. Appl.*, vol. 53, pp. 296–304, Jan./Feb. 2017.
[68] Y. Zhang, D. Xu, J. Liu, S. Gao, and W. Xu, "Performance improvement of model-predictive current control of permanent magnet synchronous motor drives," *IEEE Trans. Ind. Appl.*, vol. 53, pp. 3683–3695, Jul./Aug. 2017.
[69] L. Tarisciotti, J. Lei, A. Formentini, A. Trentin, P. Zanchetta, P. Wheeler, and M. Rivera, "Modulated predictive control for indirect matrix converter," *IEEE Trans. Ind. Appl.*, vol. 53, pp. 4644–4654, Sep./Oct. 2017.
[70] F. Donoso, A. Mora, R. Cárdenas, A. Angulo, D. Sáez, and M. Rivera, "Finite-set model predictive control strategies for a 3L-NPC inverter operating with fixed switching frequency," *IEEE Trans. Ind. Electron.*, vol. 65, pp. 3954–3965, May 2018.
[71] P. Karamanakos, R. Mattila, and T. Geyer, "Fixed switching frequency direct model predictive control based on output current gradients," in *Proc. IEEE Ind. Electron. Conf.*, (Washington, D.C.), pp. 2329–2334, Oct. 2018.
[72] C. Zheng, T. Dragičević, B. Majmunović, and F. Blaabjerg, "Constrained modulated-model predictive control of an LC-filtered voltage source converter," *IEEE Trans. Power Electron.*, pp. 1–11, in print, 2019, DOI: 10.1109/TPEL.2019.2917634.
[73] V. Yaramasu, B. Wu, and J. Chen, "Model-predictive control of grid-tied four-level diode-clamped inverters for high-power wind energy conversion systems," *IEEE Trans. Power Electron.*, vol. 29, pp. 2861–2873, Jun. 2014.
[74] V. Yaramasu and B. Wu, "Predictive control of a three-level boost converter and an NPC inverter for high-power PMSG-based medium voltage wind energy conversion systems," *IEEE Trans. Power Electron.*, vol. 29, pp. 5308–5322, Oct. 2014.
[75] A. Ayman, P. Karamanakos, and R. Kennel, "Direct model predictive current control strategy of quasi-Z-source inverters," *IEEE Trans. Power Electron.*, vol. 32, pp. 5786–5801, Jul. 2017.
[76] R. Baidya, R. P. Aguilera, P. Acuña, S. Vasquez, and H. d. T. Mouton, "Multistep model predictive control for cascaded H-bridge inverters—Formulation and analysis," *IEEE Trans. Power Electron.*, vol. 33, pp. 876–886, Jan. 2018.
[77] H. Gao, B. Wu, D. Xu, and N. R. Zargari, "A model predictive power factor control scheme with active damping function for current source rectifiers," *IEEE Trans. Power Electron.*, vol. 33, pp. 2655–2667, Mar. 2018.
[78] P. Acuña, C. Rojas, R. Baidya, R. P. Aguilera, and J. Fletcher, "On the impact of transients on multistep model predictive control for medium-voltage drives," *IEEE Trans. Power Electron.*, vol. 34, pp. 8342–8355, Sep. 2019.
[79] I. Takahashi and T. Noguchi, "A new quick-response and high-efficiency control strategy of an induction motor," *IEEE Trans. Ind. Appl.*, vol. IA-22, pp. 820–827, Sep. 1986.
[80] G. S. Buja and M. P. Kazmierkowski, "Direct torque control of PWM inverter-fed ac motors—a survey," *IEEE Trans. Ind. Electron.*, vol. 51, pp. 744–757, Aug. 2004.
[81] Y. Zhang, H. Yang, and B. Xia, "Model-predictive control of induction motor drives: Torque control versus flux control," *IEEE Trans. Ind. Appl.*, vol. 52, pp. 4050–4060, Sep./Oct. 2016.
[82] P. Falkowski and A. Sikorski, "Finite control set model predictive control for grid-connected ac-dc converters with LCL filter," *IEEE Trans. Ind. Electron.*, vol. 65, pp. 2844–2852, Apr. 2018.
[83] A. Andersson and T. Thiringer, "Assessment of an improved finite control set model predictive current controller for automotive propulsion applications," *IEEE Trans. Ind. Electron.*, vol. 67, pp. 91–100, Jan. 2020.
[84] M. Dorfling, H. Mouton, P. Karamanakos, and T. Geyer, "Experimental evaluation of sphere decoding for long-horizon direct model predictive control," in *Proc. Eur. Power Electron. Conf.*, (Warsaw, Poland), pp. P.1–P.10, Sep. 2017.
[85] C. Bordons and C. Montero, "Basic principles of MPC for power converters: Bridging the gap between theory and practice," *IEEE Ind. Electron. Mag.*, vol. 9, pp. 31–43, Sep. 2015.
[86] T. Geyer and D. E. Quevedo, "Performance of multistep finite control set model predictive control for power electronics," *IEEE Trans. Power Electron.*, vol. 30, pp. 1633–1644, Mar. 2015.
[87] T. Geyer, P. Karamanakos, and R. Kennel, "On the benefit of long-horizon direct model predictive control for drives with LC filters," in *Proc. IEEE Energy Convers. Congr. Expo.*, (Pittsburgh, PA), pp. 3520–3527, Sep. 2014.
[88] T. Geyer, "Computationally efficient model predictive direct torque control," *IEEE Trans. Power Electron.*, vol. 26, pp. 2804–2816, Oct. 2011.
[89] P. Karamanakos, T. Geyer, and R. Kennel, "A computationally efficient model predictive control strategy for linear systems with integer inputs," *IEEE Trans. Control Syst. Technol.*, vol. 24, pp. 1463–1471, Jul. 2016.
[90] J.-Z. Zhang, T. Sun, F. Wang, J. Rodríguez, and R. Kennel, "A computationally efficient quasi-centralized DMPC for back-to-back converter PMSG wind turbine systems without dc-link tracking errors," *IEEE Trans. Ind. Electron.*, vol. 63, pp. 6160–6171, Oct. 2016.
[91] M. Siami, D. A. Khaburi, M. Rivera, and J. Rodríguez, "A computationally efficient lookup table based FCS-MPC for PMSM drives fed by matrix converters," *IEEE Trans. Ind. Electron.*, vol. 64, pp. 7645–7654, Oct. 2017.
[92] Y. Zhang, Y. Bai, and H. Yang, "A universal multiple-vector-based model predictive control of induction motor drives," *IEEE Trans. Power Electron.*, vol. 33, pp. 6957–6969, Aug. 2018.
[93] M. Norambuena, J. Rodríguez, Z. Zhang, F. Wang, C. Garcia, and R. Kennel, "A very simple strategy for high-quality performance of ac machines using model predictive control," *IEEE Trans. Power Electron.*, vol. 34, pp. 794–800, Jan. 2019.
[94] Y. Zhang, B. Zhang, H. Yang, M. Norambuena, and J. Rodríguez, "Generalized sequential model predictive control of IM drives with field-weakening ability," *IEEE Trans. Power Electron.*, pp. 1–12, 2019, in press.
[95] G. Mirzaeva, G. C. Goodwin, B. P. McGrath, C. Teixeira, and M. E. Rivera, "A generalized MPC framework for the design and comparison of VSI current controllers," *IEEE Trans. Ind. Electron.*, vol. 63, pp. 5816–5826, Sep. 2016.
[96] L. A. Wolsey, *Integer programming*. New York, NY: Wiley, 1998.
[97] S. A. Larrinaga, M. A. R. Vidal, E. Oyarbide, and J. R. T. Apraiz, "Predictive control strategy for dc/ac converters based on direct power control," *IEEE Trans. Ind. Electron.*, vol. 54, pp. 1261–1271, Jun. 2007.
[98] P. Stolze, M. Tomlinson, R. Kennel, and T. Mouton, "Heuristic finite-set model predictive current control for induction machines," in *Proc. IEEE Energy Convers. Congr. Expo. Asia*, (Melbourne, Australia), pp. 1221–1226, Jun. 2013.

[99] W. Xie, X. Wang, F. Wang, W. Xu, R. M. Kennel, D. Gerling, and R. D. Lorenz, "Finite-control-set model predictive torque control with a deadbeat solution for PMSM drives," *IEEE Trans. Ind. Electron.*, vol. 62, pp. 5402–5410, Sep. 2015.
[100] IEEE Std 519-2014 (Revision of IEEE Std 519-1992), "IEEE recommended practices and requirements for harmonic control in electrical power systems," Jun. 2014.
[101] M. Pacas and J. Weber, "Predictive direct torque control for the PM synchronous machine," *IEEE Trans. Ind. Electron.*, vol. 52, pp. 1350–1356, Oct. 2005.
[102] Z. Ma, S. Saeidi, and R. Kennel, "FPGA implementation of model predictive control with constant switching frequency for PMSM drives," *IEEE Trans. Ind. Informat.*, vol. 10, pp. 2055–2063, Nov. 2014.
[103] L. Tarisciotti, P. Zanchetta, A. Watson, J. C. Clare, M. Degano, and S. Bifaretti, "Modulated model predictive control for a three-phase active rectifier," *IEEE Trans. Ind. Appl.*, vol. 51, pp. 1610–1620, Mar./Apr. 2015.
[104] M. Vijayagopal, P. Zanchetta, L. Empringham, L. de Lillo, L. Tarisciotti, and P. Wheeler, "Control of a direct matrix converter with modulated model-predictive control," *IEEE Trans. Ind. Appl.*, vol. 53, pp. 2342–2349, May/Jun. 2017.
[105] R. Vargas, J. Rodríguez, U. Ammann, and P. W. Wheeler, "Predictive current control of an induction machine fed by a matrix converter with reactive power control," *IEEE Trans. Ind. Electron.*, vol. 55, pp. 4362–4371, Dec. 2008.
[106] P. Cortés, G. Ortiz, J. I. Yuz, J. Rodríguez, S. Vazquez, and L. G. Franquelo, "Model predictive control of an inverter with output LC filter for UPS applications," *IEEE Trans. Ind. Electron.*, vol. 56, pp. 1875–1883, Jun. 2009.
[107] S. Richter, S. Mariéthoz, and M. Morari, "High-speed online MPC based on a fast gradient method applied to power converter control," in *Proc. Am. Control Conf.*, (Baltimore, MD), pp. 4737–4743, Jun./Jul. 2010.
[108] H. Peyrl, A. Zanarini, T. Besselmann, J. Liu, and M.-A. Boéchat, "Parallel implementations of the fast gradient method for high-speed MPC," *Control Eng. Pract.*, vol. 33, pp. 22–34, Dec. 2014.
[109] S. Richter, T. Geyer, and M. Morari, "Resource-efficient gradient methods for model predictive pulse pattern control on an FPGA," *IEEE Trans. Control Syst. Technol.*, vol. 25, pp. 828–841, May 2017.
[110] C. M. Hackl, "MPC with analytical solution and integral error feedback for LTI MIMO systems and its application to current control of grid-connected power converters with LCL-filter," in *Proc. IEEE Int. Symp. Pred. Control of Elect. Drives and Power Electron.*, (Valparaíso, Chile), pp. 61–66, Oct. 2015.
[111] C. Dirscherl and C. M. Hackl, "Model predictive current control with analytical solution and integral error feedback of doubly-fed induction generators with LC filter," in *Proc. IEEE Int. Symp. Pred. Control of Elect. Drives and Power Electron.*, (Pilsen, Czech Republic), pp. 25–30, Sep. 2017.
[112] H. T. Nguyen, E.-K. Kim, I.-P. Kim, H. H. Choi, and J.-W. Jung, "Model predictive control with modulated optimal vector for a three-phase inverter with an LC filter," *IEEE Trans. Power Electron.*, vol. 33, pp. 2690–2703, Mar. 2018.
[113] C. Dirscherl, J. Fessler, C. M. Hackl, and H. Ipach, "State-feedback controller and observer design for grid-connected voltage source power converters with LCL-filter," in *Proc. IEEE Conf. Control Appl.*, (Sydney, NSW, Australia), pp. 215–222, Sep. 2015.
[114] T. Mouton and T. Geyer, "Trajectory-based LQR control of a grid-connected converter with an LCL filter," in *IFAC Conf. on Nonlin. Model Pred. Control*, (Madison, WI), pp. 273–278, Aug. 2018.

Petros Karamanakos (M'14–SM'19) received the Diploma and the Ph.D. degrees in electrical and computer engineering from the National Technical University of Athens (NTUA), Athens, Greece, in 2007, and 2013, respectively.

From 2010 to 2011 he was with the ABB Corporate Research Center, Baden-Dättwil, Switzerland, where he worked on model predictive control strategies for medium-voltage drives. From 2013 to 2016 he was a PostDoc Research Associate in the Chair of Electrical Drive Systems and Power Electronics, Technische Universität München, Munich, Germany. Since September 2016, he has been an Assistant Professor in the Faculty of Information Technology and Communication Sciences, Tampere University, Tampere, Finland. His main research interests lie at the intersection of optimal control, mathematical programming and power electronics, including model predictive control for power electronic converters and ac drives.

Dr. Karamanakos received the 2014 Third Best Paper Award of the IEEE Transactions on Industry Applications and the First Prize Paper Award of the Industrial Drives Committee at the 2013 IEEE Energy Conversion Congress and Exposition.

Tobias Geyer (M'08–SM'10) received the Dipl.-Ing. and Ph.D. degrees in electrical engineering from ETH Zurich, Zurich, Switzerland, in 2000 and 2005, respectively, and the Habilitation degree in power electronics from ETH Zurich, Zurich, Switzerland, in 2017.

After his Ph.D., he spent three years at GE Global Research, Munich, Germany, and another three years at the University of Auckland, Auckland, New Zealand. In 2012, he joined ABB's Corporate Research Centre, Baden-Dättwil, Switzerland, where he is currently a Senior Principal Scientist for power conversion control. He was appointed as an extraordinary Professor at Stellenbosch University, Stellenbosch, South Africa, from 2017 to 2020.

He is the author of more than 130 peer-reviewed publications, 30 patent applications, and the book "Model predictive control of high power converters and industrial drives" (Wiley, 2016). He teaches a regular course on model predictive control at ETH Zurich. His research interests include medium-voltage and low-voltage drives, utility-scale power converters and model predictive control.

Dr. Geyer is the recipient of the 2017 First Place Prize Paper Award in the Transactions on Power Electronics, the 2014 Third Place Prize Paper Award in the Transactions on Industry Applications, and of two Prize Paper Awards at conferences. He is a former Associate Editor for the Transactions on Industry Applications (from 2011 until 2014) and the Transactions on Power Electronics (from 2013 until 2019). He was an international program committee vice chair of the IFAC conference on Nonlinear Model Predictive Control in Madison, WI, USA, in 2018.